Final Report

Advanced S-Band Studies Using the
TDRSS Communications Satellite

NASA Grant NAG-5-2142

NASA Headquarters
Greenbelt, MD
August 23, 1994

submitted by

Mr. Jeffrey D. Jenkins
Dr. William P. Osborne
Mr. Yiping Fan

New Mexico State University
Dept. Of Electrical Engineering
Las Cruces, NM 88003

Table of Contents

List of Figures

List of Tables

1. Introduction

This report will detail the results of a propagation experiment to measure the statistics of the fading channel for spread spectrum mobile satellite communication links. However, before the experiment is presented, it is useful to examine the bigger picture of mobile communication systems in general. Through an understanding of the role that spread spectrum plays in this bigger picture, the motivation for the current research becomes clear.

Mobile communications are important because we live in a highly mobile society. There is a demand for low cost high performance personal communcations devices for phone, paging, messaging, and navigation. The businessman who must travel to meet with clients has a need to maintain contact with his main office. The family who wishes to vacation in the mountains may enjoy the ability to contact friends without the need to drive into the nearest town for a telephone. Aircraft and ships in distress may require the ability to accurately relay their positions to rescue workers no matter where on the earth they are at. To succeed in the market place, these communications devices must operate reliably in whatever environment the end user desires to use them in. It is unlikely that any system which demands the end user to only operate the device under strict preconditions would ever become widespread in use.

The last five years have seen the rapid growth in the cellular telephone industry. It is now commonplace for families and businessmen alike to have telephones in their cars. As this technology has reached the general consumer, the demand has grown to increase the availability and coverage provided by these services. In addition, as the public has become aware of the capability of new technologies, markets have been opened in new paging and messaging services that achieve continental coverage through the use of earth-orbiting satellites. The United States governement navigation system known as the Global Positioning System (GPS), has been being placed into operation since 1983, and the unprecedented accuracy and global coverage of this system for navigation and surveying has resulted in a great deal of interest in similar systems for both civilian and government use. This interest resulted in the definition of a new class of service by the Federal Communications Commission (FCC) known as the Radio Determination Satellite Service (RDSS). A number of applications have been filed with the FCC to build systems using the newly allocated frequency bands.

Every communcations system that has ever been built relies on the ability to convey information across a channel from the sender to the receiver. In some cases, such as the telephone network, this channel may be a twisted pair of wires. In other cases, such

as the shortwave broadcasting service, the physical channel is the "ether", or space between transmitter and receiver, and the information is conveyed by the propagation of electromagnetic waves. From an engineering point of view, the type of physical channel is not as important as what its electrical characteristics are. Not all physical channels perform as good as others. Such is the case with mobile propagation channels. Unlike a twisted pair of wires, or the channel between two fixed points on the earth, the mobile channel is constantly changing. In fact, the very name *"mobile propagation channel"* refers to the primary property of these channels - the path through which the signals propagate constantly changes with the location of the mobile equipment. It is important to understand the statistical properties of such channels, such as the typical attenuation, the cumulative distribution function for the channel attenuation, and how these properties vary with the terrain and orientation of the satellite with respect to the mobile equipment. Through a good understanding of these properties, it is possible to determine how reliably the system will work, and if such reliability is saleable to the consumer.

Most commercial communications devices in use by the average consumer incorporate very mature radio transmission technologies, such as Amplitude Modulation (AM) and Frequency Modulation (FM). However, there has been a shift to newer digital technologies in the last decade. Digital systems commonly employ Frequency Shift Keying (FSK) or Phase Shift Keying (PSK) to transmit bits of infomation across the channel. Digital signals also readily lend themselves to other transmission techniques, of which Spread Spectrum signalling is one. With spread signalling, the signal is transmitted using a much broader bandwidth than is required by the baseband signal. This is accomplished by employing a spreading function before the signal is transmitted. This spreading function consists of a pseudorandom sequence of bits, known as a PN sequence, which increases the bandwidth of the signal. Such a technique provides many benefits, which include performance gains against interfering signals or jammers, the ability to peacefully coexist on a channel with other spread signals employing orthogonal spreading functions (Code Division Multiple Access, or CDMA), and the ability to derive more accurate bit time references. Navigation systems, such as GPS, make use of the time references to improve system accuracy, and in times of crises, the government enjoys the improvement against malicous jamming of the system. These are some of the reasons why spread spectrum, and the propagation of spread signals, has become a topic of great interest.

The research detailed in this report arose out of an interest to better understand how the spread spectrum propagation channel may differ from the conventional channel.

Because of the wide bandwidth and ability to reject some multipath components, the spread channel should experience less fading in theory. Is this the case in practice?

This report will describe the design, implementation, and results of a propagation experiment which used TDRSS to transmit spread signals at S-Band to an instumented mobile receiver. The results consist of fade measurements and distribution functions in 21 environments across the Continental United Status (CONUS). From these distribution functions, some idea may be gained about what system designers should expect for excess path loss in many mobile environments. Some of these results may be compared against similar measurements made with narrowband beacon measurements. Such comparisons provide insight into what gains the spread signalling system may or may not have in multipath and shadowing environments.

1.1 Review of Previous Work

NASA Reference Publication 1274 [1] contains a complete and detailed survey of the previous work done in mobile propagation experiments through 1992. While it is not the purpose of this document to duplicate this effort, it is instructive to highlight some of these previous experimental efforts. In particular, all of the experiments in mobile propagation that are described in [1] have employed CW beacons as signal sources. More recently, a few experiments have been performed with spread signalling, with the objective being to measure delay spreads in urban environments. This work will also be summarized below.

CW Experiments

The previous propagation experiments have examined many aspects of mobile satellite propagation. Experiments in the mid '80's by Vogel and Goldhirsh [2], measured the fading caused by single trees, and looked at how the fade statistics varied with the type of tree. With the signal source located on a tower, only a single elevation angle could be tested. In these same series of experiments, fades were measured at both UHF (870 MHz) and at L-Band, and the effects of frequency on fading were examined. The results from these studies were worst case and median attenuation values for several tree species, as well as a frequency scaling model to predict what the attenuation might be in other bands of interest.

Later measurements by Vogel and Goldhirsh [3] examined how the attenuation from single trees varied with elevation angle to the signal source. By using a helicopter as a platform, the fade statistics could be measured at several elevation angles. Measurements were repeated with and without foliage by testing in the summer and winter months. The results from these measurements were models which could be used to estimate the attenuation at any elevation angle for a given tree.

The measurements above involved single trees in a static situation. Other work was done for the mobile case, where fade statistics were gathered as the experiment was moved through many different trees. In [4], the results of a series of such measurements was reported, and an empirical model given which predicts the fade statistics in a roadside tree environment. This model has become known as the Empirical Roadside Shadowing model, and has been validated within a few dB by other researchers [5]. This model was developed from L-Band propagation data, and is only valid over elevation angles from 20 to 60 degrees, and for a limited portion of the total fade distribution curve.

In 1988, Vogel and Goldhirsh [6] reported on the results of a measurement campaign in mountains and canyons. These were environments where multipath fading was expected to be present. These measurements were made at 870 MHz and 1500 MHz, and resulted in more empirical curve fits to predict fade distributions in multipath environments similar to those tested. These curves again have only limited applicability, and are valid over limited portions of the total fade distribution range. No elevation angle dependance has been determined for these measurements.

Most recently, Vogel has reported [7] on an experiment underway to employ two signal sources with a varying angular separation, and directly measure the diversity gains available as a function of the angular separation between sources. No results from these experiments has been published as of this writing.

Spread Measurments

Since 1992, there have been two experiments reported utilizing spread spectrum signalling to measure propagation effects. In the United States, Ghassemzadeh et al. [8] have reported an experiment which measured delay spreads and fade statistics for a spread system with varying chip rate. These measurements were limited to inside buildings and on the sidewalks of downtown Manhattan in New York. This research showed that the observed fades were reduced with increasing chip rate. With the dominant source of fading being multipath, it is expected that the spread system with the higher chip rate would have a higher probability of rejecting close-in multipath. Unfortunately, this series

of experiments did not examine the performance of spread signalling in other geographical locations of interest.

In Japan, researchers have been using the ETS-V satellite as a signal source, and have been investigating the performance of an L-Band spread system [9]. It should be noted that this experiment was not intended to collect propagation data, but rather to verify that their new spread system was operating properly. In this experiment, a spread signal carrying data was transmitted along with a CW beacon to a mobile receiver driving in suburban Kashima. At the receiver, bit error rates were recorded and averaged over 1 and 30 second intervals, and these error rates compared with predictions based on a Rician fading model. The authors report good correlation between fades on the CW beacon and increased BER on the spread channel. They also have reported that the BER performance agrees well with that predicted for a non-selective Rician fading channel with K=12.

No data has been published that gives the fade statistics for a spread spectrum system in typical operating environments. In particular, no measurements have been made in open areas, mountainous areas, or along tree-lined roads. Each of these environments will have its own mix of multipath and shadowing effects, with the delay spreads of the multipath different from region to region. While theory predicts that spread signalling performs better in the presence of separable multipath, no work has been done until now to actually see how spread systems *do* perform in typical operating environments. That is what the experiment described in this report is about.

This report has been divided into three main chapters dealing with experiment design, data collection, and comparisons with unspread propagation data. Chapter 2 is devoted to describing the design, fabrication, and validation testing of the experimental apparatus. This discussion includes software issues as well as the hardware. Chapter 3 gives the details of how and where propagation data was collected, and sumarizes the cumulative fade distributions resulting from these measurements. Chapter 4 takes a look at how the spread fade distributions compare with some of the narrowband beacon measurements published by other researchers.

2. Wideband Propagation Measurement System

2.1 Introduction

This wideband propagation measurement system consisted of a hardware system and a software system. In Section 2.2, the configuration and operation of the hardware system is described. The hardware system was comprised of a transmitter, located at White Sands Ground Terminal (WSGT), a receiver and a data acquisition in a van. The software and its operation is discussed in Section 2.3. Section 2.4 is devoted to the evaluation and validation of both hardware and software systems. Section 2.5 is a summary of Chapter 2.

System design and parameter selection were based upon the availability of resources and system components (especially upon a surface acoustic wave matched filter supplied by Mobile Datacom Corporation) as well as link budget analysis. According to available information, the link budget analysis is given in Table 1. It is indicated that in a typical operating enviromentthe available E_s/N_0 is 26.1 dB. With the minimum E_s/N_0 required for signal detection of 5 dB, the resulting dynamic range of the measurement is 21.1 dB. This dynamic range was confirmed by the tests in Section 2.4 with only about one dB difference.

EIRP @ TDRS-F3	+ 47 dBW
Receiver Antenna Gain	+ 5.0 dBic
Free Space Path Loss @ 2090 MHz	- 191.8 dB
Carrier Power @ Ground	- 139.3 dBW
Antenna Temperature	300 K
LNA Temperature	124 K
System Temperature	235 K
kTsys	- 204.9 dB
C/kT	+ 65.6 dB
Symbol Rate	+ 39 dB
Es/No	+ 26.1 dB
Minimum Es/No for Detection	+ 5 dB
Dynamic Range	+ 21.1 dB

Table 1. Link budget

2.2 Hardware System

2.2.1 Transmitter

The transmitter hardware, located at White Sands Ground Terminal (WSGT), consisted of a PN-generator with an 8 MHz clock and a BPSK modulator. The general block diagram is shown in Figure 2.1.

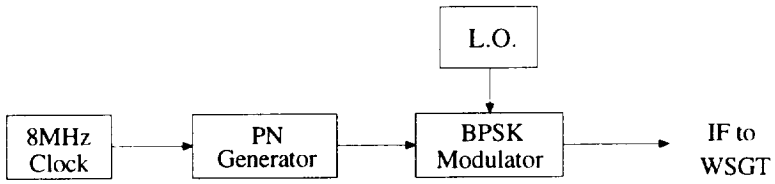

Figure 2.1 Block Diagram of Transmission Equipment

The PN generator produced a 1024 chip sequence to match that of the SAW matched filter at the receiving end. This sequence consisted of four 256 bit code sequences in a non-inverted/inverted/non-inverted/non-inverted pattern. This means that the first sequence of 256 chips is non-inverted code; the second one is the same code sequence, but inverted; the third and fourth 256 chip blocks are identical to the first sequence.

This 1024 chip sequence, driven by the 8MHz clock, was input to the BPSK modulator working at an intermediate frequency (IF) of 370.000 MHz to provide a spread spectrum signal operating at 8 MChips/sec with null-to-null bandwidth of 16 MHz. This spread spectrum signal was transmitted to TDRS-F3 by the WSGT at K-band unlink and received by the mobile receiver at S-band (2090 MHz) via the TDRS-F3 satellite downlink. WSGT transmitted the 1024 chip sequence continuously for the duration of the test.

2.2.2 Receiver

The receiver hardware set in the van consisted of a Quad Helix antenna, an S-band receiver, a SAW matched filter, and an envelope detector. The general block diagram of the receiver subsystem is depicted in Figure 2.2. The S-band receiver unit mixed the received signal with the proper frequencies to bring the signal down to an intermediate frequency matching that of the SAW matched filter. The envelope detector converted the output of the matched filter into a baseband signal which was fed to the data acquisition system (DAS) for digitizing, sampling and data storage.

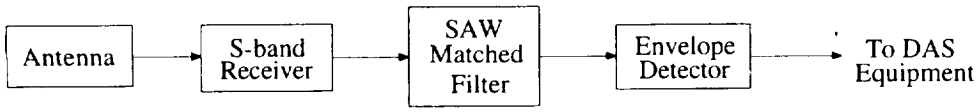

Figure 2.2 Block Diagram of Receiver Equipment

Antenna

The antenna subsystem, mounted on the roof of the van, was composed of a Quad Helix antenna and a low noise amplifier (LNA). The Quad Helix antenna was selected to obtain omnidirectional coverage. It had a left hand circular polarization and a peak gain of 5 dBic. To minimize the SNR degradation due to cable loss between the antenna and the S-band receiver, a low noise amplifier with 20 dB gain was mounted immediately following the antenna.

Figures 2.4(a)-(c) show the electric field patterns of the antenna where the antanna was evaluated with fixed incident angles (15°,30° and 45°) and a varying rotation angle from 0° to 360° (Case one). In contrast, Figures 2.6(a)-(b) depict the electric field patterns where the antanna was evaluated with fixed rotation angles (0° and 90°) and a varying incident angle from 0° to 360° (Case two). Figure 2.3 and Figure 2.5 picturoly demonstrate how the antenna evaluation was done for the above two cases. These antenna patterns were sufficient to cover all likely driving conditions in the data collection campaign.

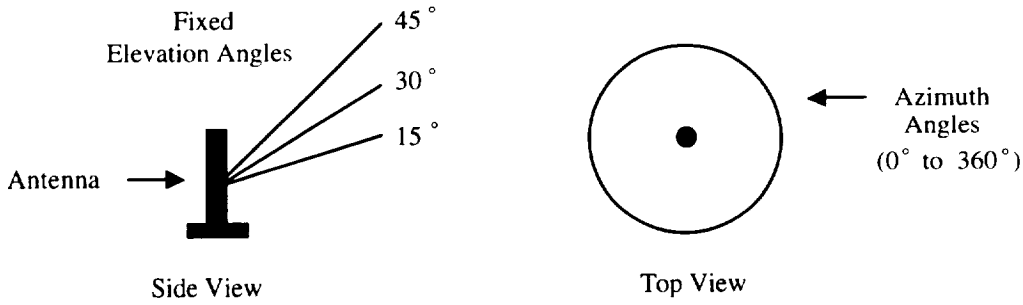

Figure 2.3 Antenna Pattern Evaluation for Case One

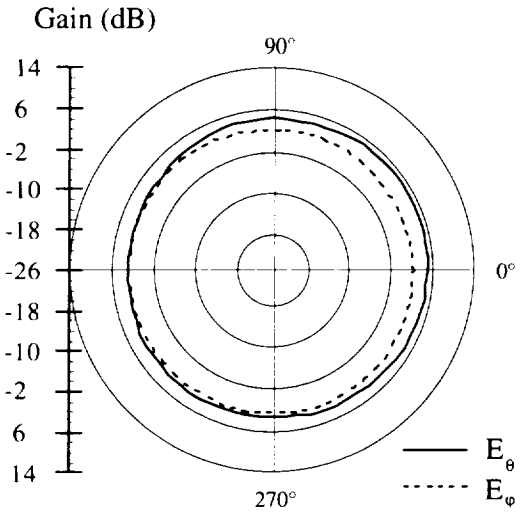

(a) incident 15° and rotation 0° – 360°

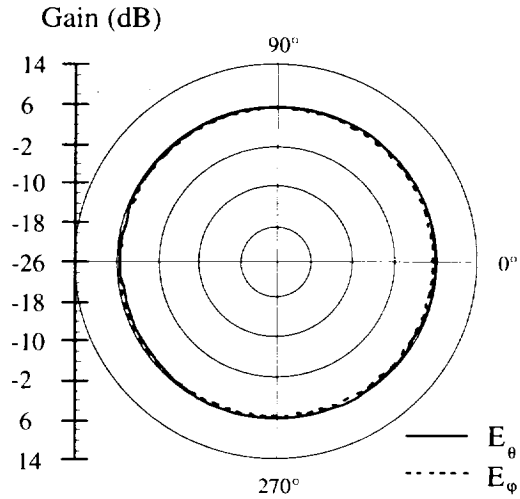

(b) incident 15° and rotation 0° – 360°

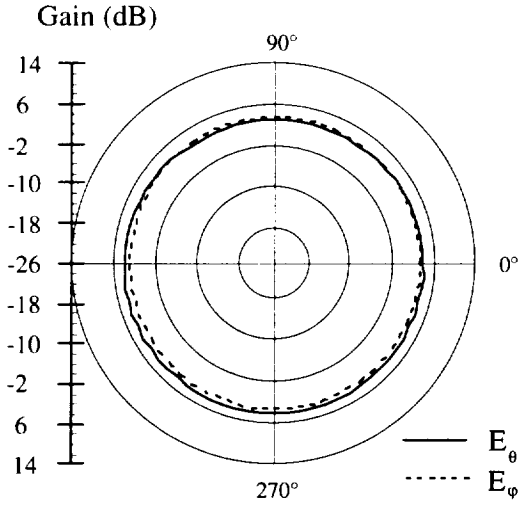

(c) incident 45° and rotation 0° – 360°

Figure 2.4 Antenna Patterns for Case One

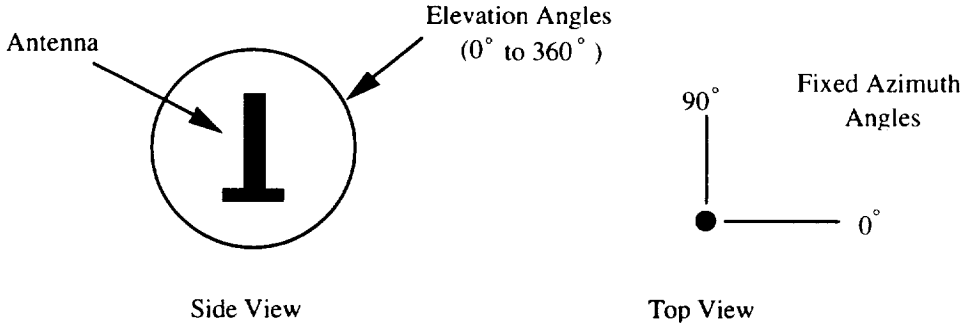

Figure 2.5 Antenna Pattern Evaluation for Case Two

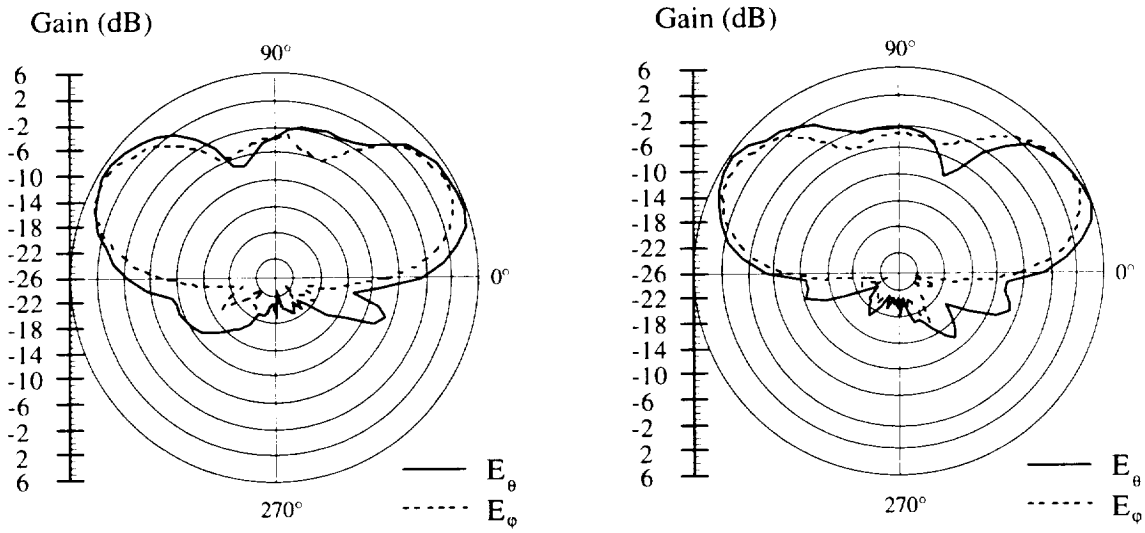

(a) incident $0^\circ - 360^\circ$ and rotation 0° (b) incident $0^\circ - 360^\circ$ and rotation 90°

Figure 2.6 Antenna Patterns for Case Two

S-Band Receiver

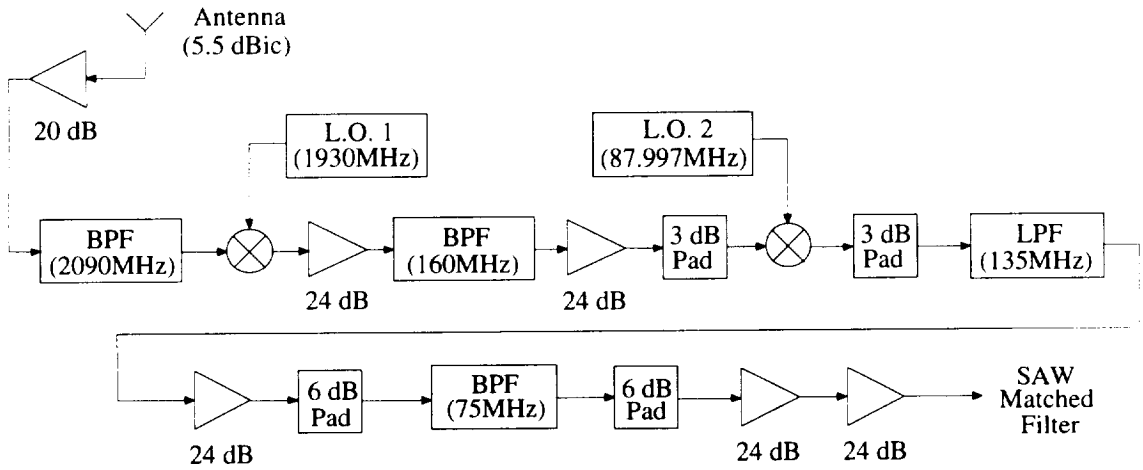

Figure 2.7 S-Band Receiver Block Diagram

The S-band receiver contained the down-conversion hardware as shown in Figure 2.7. The S-band signal from TDRS-F3 was received through the Quad Helix antenna and entered a band pass filter (BPF) centered at 2090 MHz to reject out-band noise. The output of the BPF was mixed with a 1930 MHz source from L.O. 1 (HP8657B signal generator), and a second BPF was used to pass the desired frequencies centered at 160 MHz. The signal was mixed a second time, with 87.997 MHz supplied by L.O. 2 (HP-8656B signal generator). A 135 MHz low pass filter (LPF) was used to reject the mixer

product of 247.997 MHz. The signal was then band-pass filtered at 75 MHz to isolate the required frequencies (centered at 72.003 MHz, i.e., the IF frequency of the SAW matched filter) of the mixer. This resulting signal was fed into the SAW matched filter. Several amplifiers and pads were used to provide isolation and the desired signal gain.

SAW Matched Filter

The SAW matched filter converted the modulated PN sequence to an IF autocorrelation pulse. This special matched filter was comprised of four SAW sub-filters (see Figure 2.8). Each sub-filter matched the same 256-chip sequence of non-inverted Gold code. Functionally, the third sub-filter matched to the 256-chip sequence of inverted Gold code, because of its negative contribution to summer. This structure theoretically ensured that (1) when each sub-filter aligned with this 256-chip sequence and the received sequence pattern was non-inverted/inverted/non-inverted/non-inverted, the output of the matched filter would produced an IF autocorrelation pulse of width 250 ns, and (2) when either the pattern or the 256-chip sequence was misaligned, no output or noise with very small magnitude, would be generated. Figure 2.9 shows a typical output of the SAW matched filter in response to the 1024 PN sequence after the demodulation by the envelope detector. Since the DAS sampled only 1000 points per waveform at 50 MSa/s, Figure 2.10 shows a fraction (20 μs out of 128 μs) of the response around the auotcorrelation pulse. In Figure 2.9, a more detailed block digram of the SAW matched filter is given.

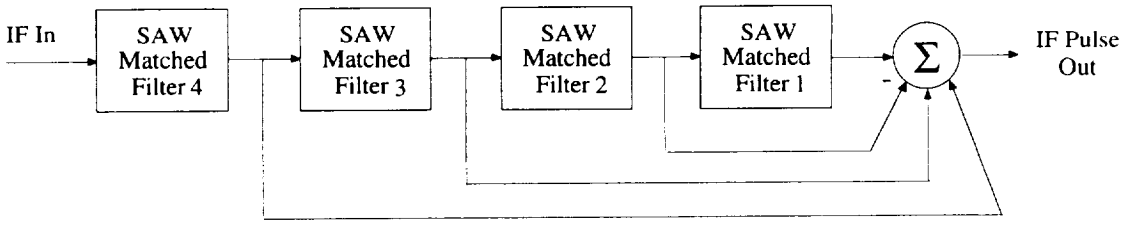

Figure 2.8 Matched Filter Configuration

Envelope Detector

The IF output of the SAW matched filter was demodulated with the HP model 420B envelope detector. Because this particular envelope detector provided a negative pulse, it was inverted and then amplified to provide a baseband autocorrelation pulse.

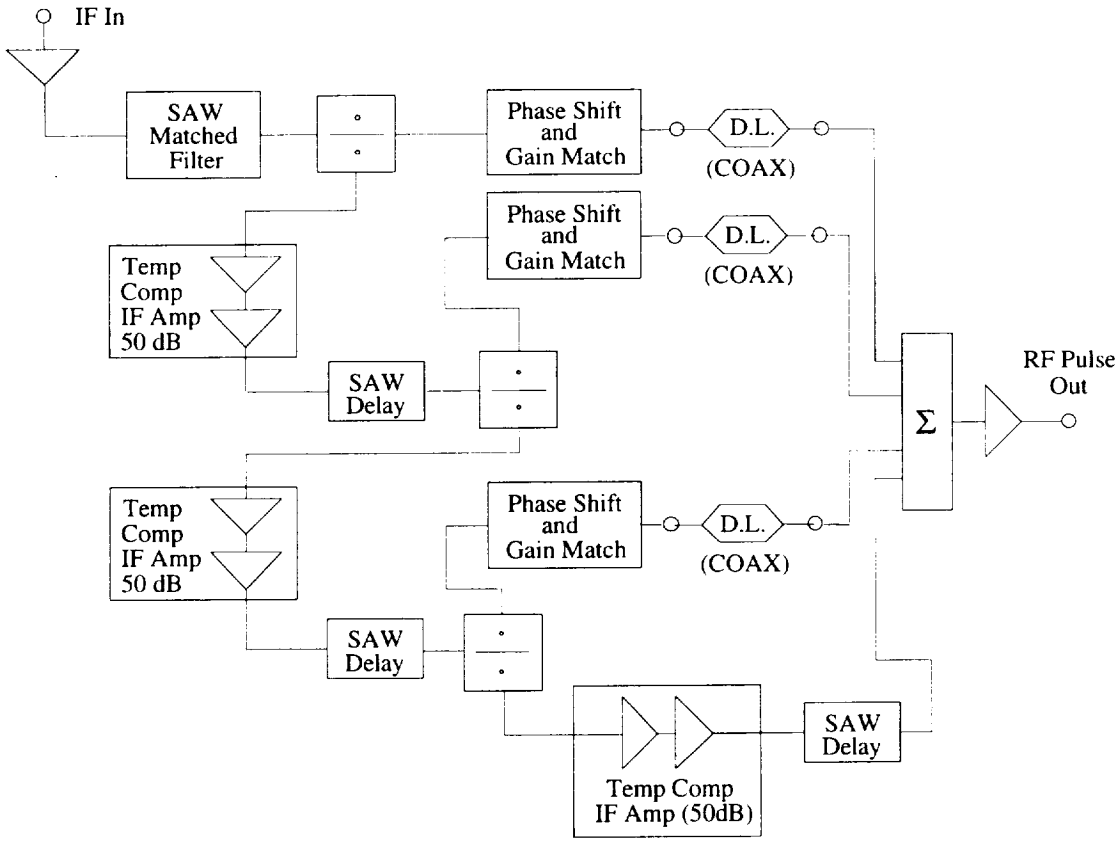

Figure 2.9 Detailed Configuration of the SAW Matched Filter

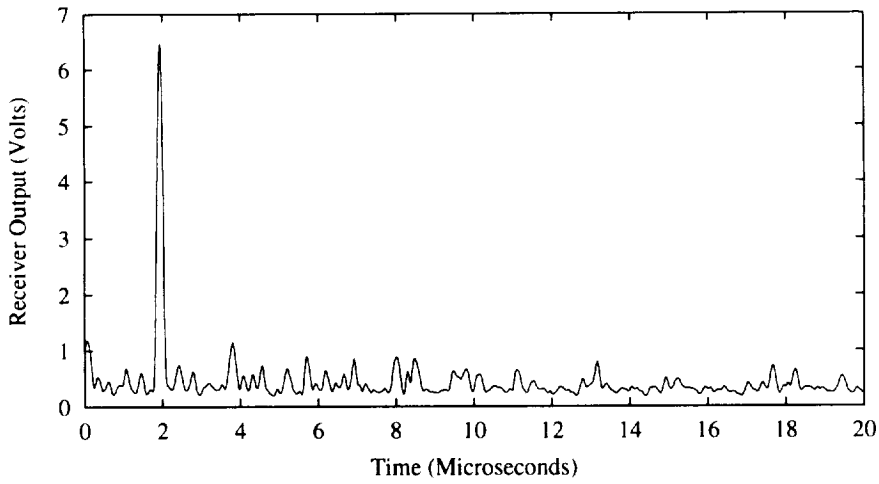

Figure 2.10 Typical Response of the Matched Filter

2.2.3 Data acquisition system

The DAS was responsible for the digitization, sampling and storage of the output of the SAW matched filter. Some basic functions of the DAS were:

1) Digitize, sample and store waveforms;
2) Acquire GPS data every minute;
3) Determine the synchronization state or lock condition;
4) Record multipath signals with maximal differential distance of 3 miles.

The autocorrelation pulse to be digitized was 250 ns wide (two-times the bit duration at 8 Mchips/sec). The pulse was sampled at 50 MSa/s. This gave 12 samples along the autocorrelation pulse to allow pulse reconstruction and peak estimation.

Objects within a few miles are of concern because they may cause significant multipath interference in received signals. Multipath signals from objects farther than a few miles away are attenuated to atmospheric noise levels and are therefore not necessary to observe. It was necessary to digitize enough points so that a total multipath differential distance (distance traveled by the multipath signal minus that traveled by the direct signal) of several miles was included in the waveform record. At a sample rate of 50 MSa/s, a waveform with 806 samples was able to see a multipath distance less than or equal to 3 miles. For simplicity, the number of samples per waveform was selected to be 1000 which resulted in a total of 20 μs of data per waveform. Accounting for 2 μs of data, collected prior to the peak (Figure 2.11), a total of about 18 μs was left for the autocorrelation pulse and multipath. Hence, the multipath effect which could be seen from the waveform had a maximal distance of 3.35 miles.

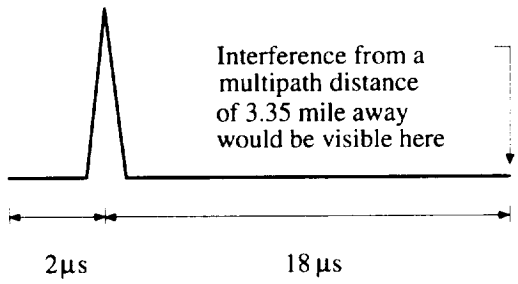

Figure 2.11 Theoretical Received Waveform

The DAS consisted of a frame synchronizer, a GPS antenna, a GPS receiver card, an HP digitizing oscilloscope, IEEE-488 interface card, a 486-33 MHz computer and a tape backup system. A video camcorder was also present to record actual paths traversed by the van. This allowed us in part to review weather conditions and objects causing interference in data analysis. A general block diagram of the DAS equipment is shown in Figure 2.12. The software used in DAS is described in the Software Section.

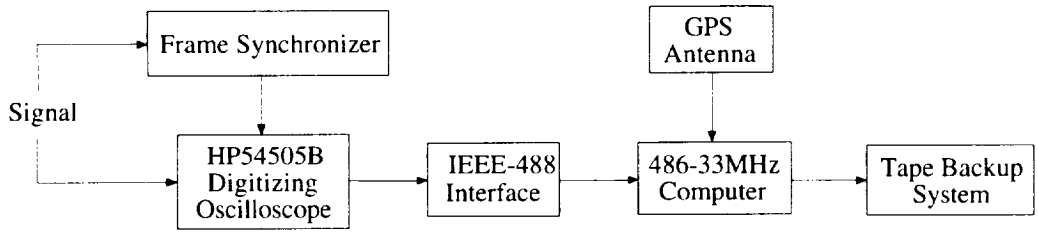

Figure 2.12 Block Diagram of the DAS

Frame Synchronizer

The baseband autocorrelation pulse from the envelope detector was supplied to the frame synchronizer. The frame synchronizer board used a digital phase locked loop design to acquire and track a pulse of known period. The circuit then provided an external trigger pulse to the oscilloscope signifying both the lock condition of the board and the imminent occurrence of the tracked pulse within a known window of time so that data could be sampled. Figure 2.13 is a block diagram of the frame synchronizer.

In a locked condition, the incoming pulse occurred within a "look" window. If the pulse was away from the center of the window, a feedback mechanism was involved such that the VCO input voltage was altered which forced the center of the window tracking the incoming pulse. Board timing was derived from two counter circuits. The first circuit operated at 16 MHz and consisted of a 24 bit counter used to set the desired pulse period. The second counter circuit operated at 2 MHz and adjusted the length of the window.

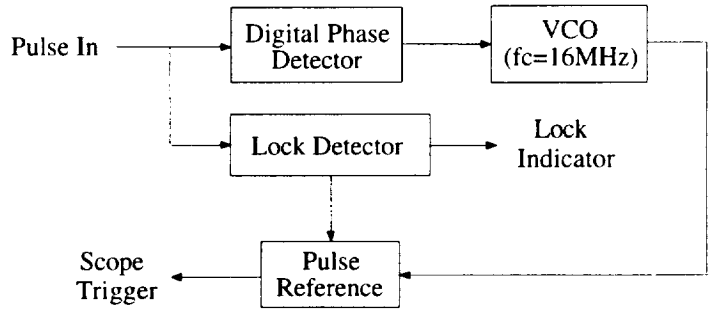

Figure 2.13 Frame Synchronizer Block Diagram

The look window period (Figure 2.14) was selected to be 128 μs which was the elapsed time between autocorrelation pulses generated by the matched filter. The window duration was selected to be 4 μs, 16 times the pulse width of 250 ns.

The lock detector circuit was also built to indicate the lock condition. The lock condition remained in effect as long as pulses in the window occurred. This sustained lock

allowed the system to momentarily lose the incoming pulse and still maintain the same location in time to find it when it came back (should it be lost due to a short duration fade). The maximum time to remain in lock without a pulse was approximately 20 ms. When the circuit was out of lock, any pulse occurring within the window reset the period counter and lock was instantaneously achieved.

GPS Antenna

The GPS antenna allowed the NOVATEL Model 711 GPS receiver card, located inside the computer, to receive data from the GPS satellites. The GPS receiver card gave GPS time, latitude, longitude, altitude and standard deviations of those measurements.

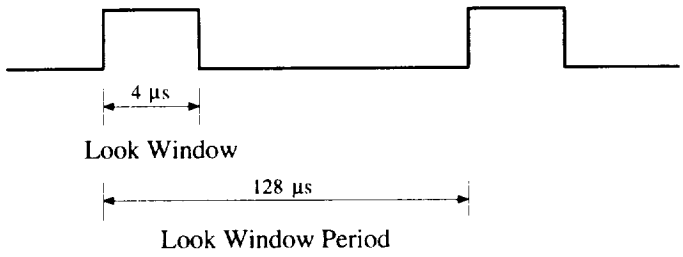

Figure 2.14 Frame Timings

HP Digitizing Oscilloscope

The HP54505B digitizing oscilloscope sampled the auto-correlation pulse from the envelope detector in the receiving equipment. The trigger pulse created by the frame synchronizer was fed directly into the scope trigger input. The 486-33MHz computer controlled the digitization process via IEEE-488 interface. The HP54505B digitizing oscilloscope was selected due to its 125 MHz bandwidth, 500 MSa/sec maximum sample rate and versatility.

486-33 MHz PC

The 486-33MHz computer with 32 Mbytes of RAM, controlled the digitization, collection, and storage of waveform data. It also controlled the collection and storage of GPS data. The computer was specifically fabricated for this project. The basic requrements were speed, large disk drive space with superior shock ratings, large RAM area and rack mounting capability for mobile unit integration. The final product consisted of a 486-33 MHz computer with two 213 MByte hard drivers and 32 MBytes of RAM, so as to accommodate the operating system, software, C compiler and 4 hours worth of digitized waveform data.

Keithly/Metrabyte IEEE-488 Interface (KPC-488.2AT)

This IEEE-488 interface card was selected for its high data transfer rate capabilities. The interface contained special hardware and used 16 bit I/O operations to achieve rates of over 1 MByte per second. It can receive up to 64KBytes of binary data in the high speed mode, limiting the number of transferred waveforms.

Tape Backup System

The tape backup system was the Colorado Jumbo 250 MByte Tape drive and software. This was used to back-up the hard drive data at the end of each days measurement. It was necessary to clear the hard drives of all waveform data before a new data run could be executed.

2.3 Software System

The software syetem controls the digitization, collection and storage of the autocorrelation pulse from the envelope detector. It also requests and collects GPS data. Since it was used in DAS, it is refer to DAS software in the following text. All source code was created in C. The GPS data collecting portions were edited from code provided by NOVATEL. A general block diagram of program flow is shown below in Figure 2.15.

2.3.1 GPS software

The GPS software package provided by NOVATEL operates with user prompts to receive GPS information. This could not be directly incorporated with the DAS control software due to required user querries. In order to meet the automated data collection requirement, the additional GPS software were developed. This will allow the waveform collection software access to GPS data without the system pausing for user inputs. NOVATEL provided the code for it's software, so reverse-engineering was applied to tailor their package to NMSU's needs.

2.3.2 Oscilloscope software

In order to store a waveform record 1000 points long, the scope must be operated in "Rawdata" mode. This is because other storing techniques will only allow 500 or 8000 point waveform records. The "Rawdata" mode acquires data with special routines that are optimized for quick unloading. While acquiring data in the Rawdata mode, data is stored

as uncalibrated 8-bit Gray code form in a large buffer. When all acquisitions are complete, the buffer is translated into unfiltered calibrated 16-bit binary data and sent over the bus in the WORD format. In the WORD format, the number of data bytes is twice the number of data points. The WORD format also assists the control software in the fact that the information can be read directly into an integer array.

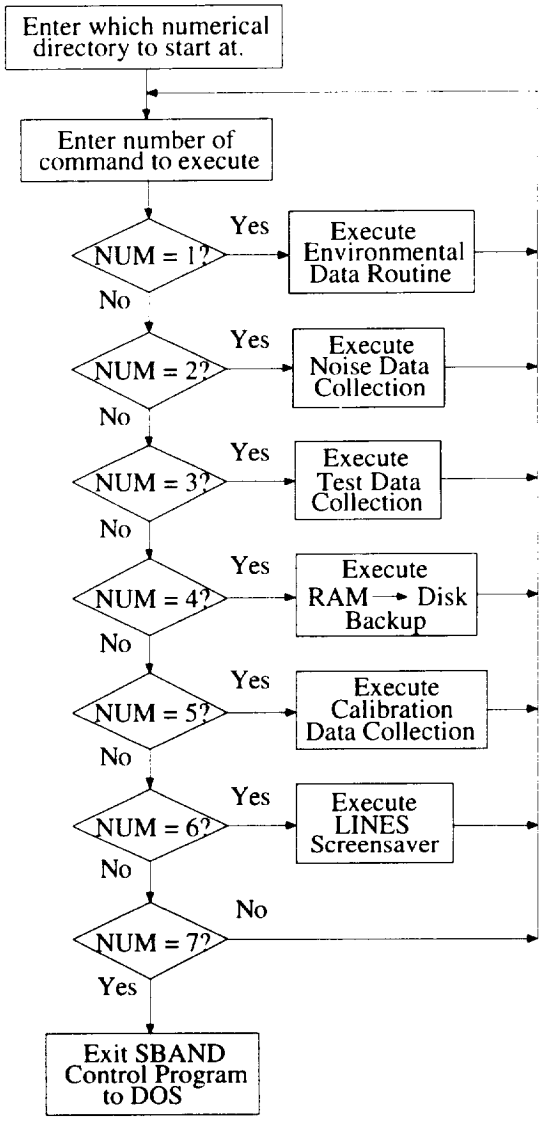

Figure 2.15 General Block Diagram of DAS Software

The waveform data is sent from the oscilloscope to the computer with the command ":WAVEFORM:DATA?". The data is transferred from the oscilloscope in a single IEEE 488.2 data block. The number of bytes in the block can be determined with the following equation: #Bytes = Acquisitions×(Length×2 + 8). The data block consists

of two arrays. The first array consists of double precision 64-bit floating point numbers. This array contains the XORIGIN values of the waveform records to follow. The second array consists of 16-bit integer numbers. This data is transmitted in a linear fashion over IEEE-488. It starts with sample zero of the first acquisition and continues through SAMPLE LENGTH - 1 of this acquisition. Then it continues in a similar fashion with sample zero through SAMPLE LENGTH - 1 of each of the following acquisitions to the last acquisition.

Because of the 64KByte block length limitation of the KPC-488.2AT interface card, the fixed record length of 1000 points/waveform and the WORD format, only 30 waveform acquisitions at 50 MSa/sec can be taken before a data transfer is required. This is because a single acquisition data block contains:

Block header:	10 Bytes consisting of binary block length
XORIGIN value:	8 Bytes (64 bit floating point number)
Data:	1000 Points X 2 Bytes/Point (WORD format) equals 2000 Bytes
TOTAL BLOCK LENGTH:	2018 Bytes for 1 waveform

Table 2.1 Single Acquisition Data Length

For 30 waveform acquisitions, the total block length would be 60,250 Bytes according the following table.

Block header:	10 Bytes (same as single block)
XORIGIN value:	30 X 8 Bytes = 240 Bytes
Data:	30 X 1000 X 2 = 60,000 Bytes
TOTAL BLOCK LENGTH:	60,250 Bytes for 30 waveforms

Table 2.2 30 Waveform Data Length

If 31 waveforms were to be collected, the 64KByte block length constraint would be exceeded.

2.3.3 Computer software

Writing to the hard drives while in transit could damage them. To overcome this problem, 28 Mbytes of RAM was configured into virtual RAM drives. With the Quarterdeck memory manager software, the largest configurable size of a RAM drive was 4096 KBytes, so 7 virtual drives (each with 4 Mbytes) were created. It took 3 seconds to digitize, transfer and store 30 waveforms and took about 20 minutes to fill all 7 RAM

drives with data. After 7 RAM drives were full of waveform data, the DAS prompted the user to stop the van so that a safe transfer from volatile RAM to the hard drive could be executed.

To provide a means of determining when the signal has been lost due to shadowing and/or multipath, the following scheme was used. After the block of 30 waveforms was digitized and collected, the computer time was recorded. The time-stamp and GPS number was store, followed by the 30 waveformss. When the time between two consecutive stamps was longer than three seconds, the signal had been lost.

Because GPS data was collected every minute, a means to correlate the GPS information to waveform record was required. A CPU time and GPS number was introduced in the data format (Figure 2.16) to achieve this correlation. At the beginning of a collection, the GPS number was zero and GPS data was collected, followed by a number of groups of 30 waveforms. Each time a new group of 30 waveforms was collected, and the elapsed time was less than 60 seconds, the GPS number was incremented. When 60 seconds had elapsed, a new GPS fix was collected and the GPS number was reset to zero. Therefore, GPS data was directly correlated to the time a group of 30 waveforms was collected by noting when the GPS number was zero. Since each sample took 16 bits, one waveform record with 1000 samples occupied 2000 bytes.

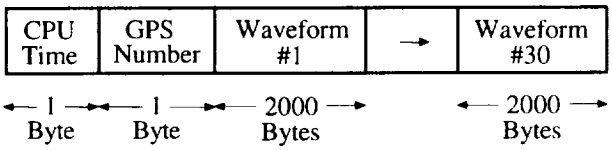

Figure 2.16 Data Format for 30 Waveforms

2.3.4 DAS software operation

It is necessary to describe a few background points before the operation can be described. The entire test period is four hours long. For each data run, 25,203,226 bytes of information is stored (includes: waveform, GPS and preamble data). The size of the **d:** hard-drive is 218Mbytes, so a total of 218M/25.2M = 8 data runs can be stored before **d:** is incapable of holding another data run. To provide a means of grouping the data collection, the following format was used: Each data run will be stored in the corresponding numerical order directory of **d:** (ie, if the second data run is being collected, it will be stored to **d:\2**; if the fourth data run is being collected, it will be stored to **d:\4**; etc.). The ninth and possible tenth data runs will be stored to **c:\extra** due to the fact that **d:** is full. If the CONTROL program is not terminated in the middle of a run, the data will

automatically be stored in the appropriate directories. However, if it is necessary to exit the CONTROL program before the four hour time period (for confirmation of data storage or any other reason), it must be noted by the user which numerical data directory the program left off at. Upon restarting the CONTROL program, simply enter the number of the directory to continue at. If a number of a directory previously used with valid data stored to it is used, that data will not be erased. However, that directory will contain two sets of data and will not necessarily represent the order in which the data was collected.

The DAS software package is executed with the following command: **control <return>** . A prompt should appear on the screen like that shown below:

[8 -> C:EXTRA directory]
Which directory to start at? (1-8)_

Enter one **1** if this is the first time the CONTROL program is executed. If it is not the first time, enter the appropriate directory to start at. After this is done, the main menu is displayed.

MAIN MENU COMMAND SCREEN

The following is displayed when the main menu is returned to:

SBAND Project Menu

1) Enter Environmental Data
2) Collect Noise Floor Data
3) Collect Test Data
4) Execute RAM->DISK backup
5) Collect Calibration Data
6) Execute LINES screensaver
7) Exit SBAND program to DOS

Enter your selection (1-7)_

Here, the appropriate commands may be executed for data collection. Type the number of the command you wish to execute.

(1) ENVIRONMENTAL DATA COMMAND

If **1** is pressed, you will see the following:

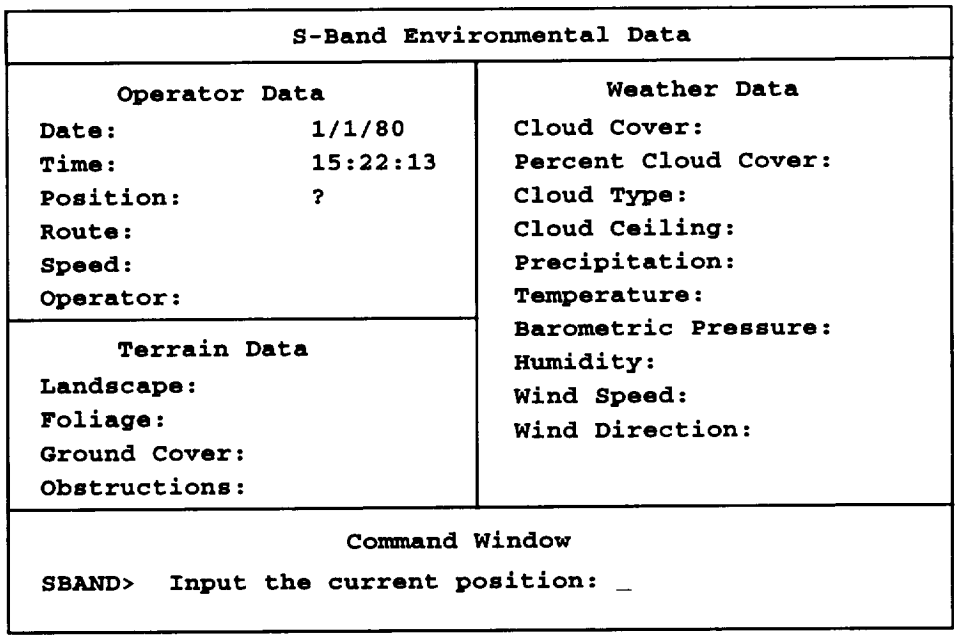

The program will prompt you through all the required environmental data. Some fields will prompt you to select a number corresponding to a particular KEY word when a infinite number of things/descriptions may be entered. Any field requiring a numerical value must be entered as an integer. Any decimal values, such as for Barometric Pressure may be entered as follows: for 30.11, enter **3011**. When all the fields are entered, you are prompted in the Command Window:

Is everything correct [Y/N]? _

Enter **N** if it is not. This will allow you to change any field you wish (or leave it the way it was by simply pressing **return**). When all is correct, pressing **Y** at the above prompt stores the data to the **d:\noise** directory with a filename as described later in the DAS software descriptions. The main menu will again be displayed and your next selection may be executed.

This information was entered shortly before the time the 4 hour test started. However, the information may be entered at a later time. What's important is that the data entered be related to the time period of the test.

(2) NOISE DATA COLLECTION COMMAND

If **2** is pressed, you will see the following:

```
                S-Band Noise Data Collection

                      Waveforms (Groups of 30)
                       1     2     3     4     5     6
                1--|--0--|--0--|--0--|--0--|--0--|--0
e:wave.out      |  G


Time Elapsed: 3

copy e:wave.out d:\noise\noise13.32
1 file(s) copied
copy e:gps.out d:\noise\ngps13.32
1 file(s) copied
copy e:preamble.out d:\noise\npre13.32
1 file(s) copied

Noise Data complete, press any key.
```

The **G** in the **e:wave.out** row and the 1 column signifies that 30 waveforms have been collected as well a GPS data. Only one group of thirty waveforms is collected. The data is automatically stored to **d:\noise**. The main menu screen is returned to and the program awaits the next command.

This collection must be executed before the test begins. It can not be executed after the transmission has begun. Doing so will simply collect 30 waveforms of test data - not noise floor data.

(3) TEST DATA COLLECTION COMMAND

If **3** is pressed, you will see the following:

Enter [1] to collect data, [2] to abort._

Entering **2** will take you back to the main menu. Entering **1** will bring up the following display:

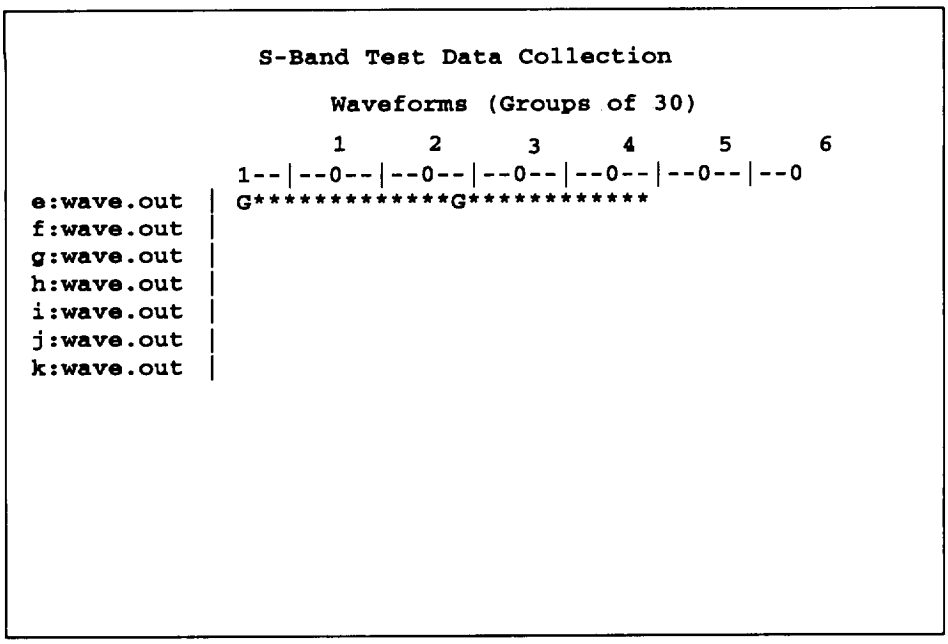

The **G**'s correspond to 30 waveforms collected with GPS data and the *'s correspond to 30 waveforms collected without GPS data. Once all 7 RAM drives are full, the program takes you back to the main menu. It is important to note that the files have not been moved from volatile RAM to DISK yet and command **4** must be executed.

If **3** is pressed and there exists RAM drive data that has not been backed up with the **4** command, you will see the following prompt:

Warning... Current data in RAMDRIVES will be erased!!!
Enter [1] to collect data, [2] to abort._

Entering **2** will return to the main menu. Entering **1** will force a data collection and the current data in the RAM drives, that has not been backed up, will be permanently erased.

After data has been collected, the main menu is returned to the screen and the program awaits the next command.

(4) RAM->DISK BACKUP COMMAND

If **4** is pressed, the following will be displayed on the screen:

Data will dump to d:\5
Enter [1] to dump data, [2] to abort._

Entering **2** will take you back to the main menu. Entering **1** will dump all RAM drive information to the corresponding numerical directory of d: drive.

If **4** is pressed and there is no current RAM drive data to be dumped, you will see the following prompt:

Warning... No current data in RAMDRIVES!!!
Data will dump to d:\5
Enter [1] to dump data, [2] to abort._

Entering **2** will return to the main menu. Entering **1** will force a data dump and the current data in the RAM drives will be stored to the corresponding numerical directory of **d:** drive.

Upon completion of backup, the main menu is returned to and the program awaits the next command.

(5) CALIBRATION DATA COLLECTION COMMAND

If **5** is pressed, the following will be displayed on the screen:

```
                S-Band Cal Data Collection

                     Waveforms (Groups of 30)
                      1     2     3     4     5     6
                 1--|--0--|--0--|--0--|--0--|--0--|--0
e:wave.out     |  G*************G************

Time Elapsed: 189

copy e:wave.out d:\cal\cal13.32
1 file(s) copied
copy e:gps.out d:\cal\cgps13.32
1 file(s) copied
copy e:preamble.out d:\cal\cpre13.32
1 file(s) copied

Cal Data complete, press any key.
```

The **G**'s signify that 30 waveforms have been collected as well a GPS data. The *'s signify that 30 waveforms with no GPS data has been collected. When a total of 60 groups of 30 waveforms has been collected, the information will be automatically stored

to **d:\cal**. The main menu screen is returned to and the program awaits the next command.

(6) LINES SCREENSAVER COMMAND:

If **6** is pressed, the LINES screensaver is executed. Simply press any key to return to the CONTROL program main menu.

(7) EXIT SBAND TO DOS COMMAND

If **7** is pressed, the CONTROL program is terminated and DOS resumes command.

SAMPLE DATA COLLECTION PROCESS

The four hour data collection process that was used for the West and South East trips consisted of the following steps:

Before Satellite transmission:

1. Have power on equipment for two hours before transmission begins. This allows ovens to warm up;
2. Locate the mobile van in a clear area for calibration data collection.
3. Enter the Environmental data;
4. Adjust the power meter for a noise floor power of 4.4 dBm;
5. Collect noise floor data;
6. Turn power meter off.

During Satellite transmission:

1. Properly tune the 2nd L.O. for maximum pulse amplitude;
2. Collect calibration data;
3. Attenuate signal so that a 3 dB enhancement will not push the pulse off the oscilloscope scale (8 Volts maximum);
4. Drive van and collect data;
5. Stop van when data has filled RAM drives to transfer to hard drive (This may be done in-transit, if the roads are smooth or if vehicle speed is reduced due to traffic);
6. Repeat 4 and 5 until four hour time window is up;

7. 10 minutes before transmission ends, find clear spot for post-calibration data collection;
8. Collect calibration data;
9. Re-tune 2nd L.O. due to temperature drifts;
10. Collect calibration data.

After Satellite transmission:

1. Collect post-noise floor data at old 2nd L.O. frequency;
2. Adjust attenuator until 4.4 dBm is read on the power meter at the re-tuned frequency;
3. Collect post-noise data;
4. Transfer disk drive data to tape backup.

2.4 System Test

Once the transmitter, receiver and data acquisition system were constructed, in-lab tests were conducted to confirm proper operation and to examine system performance. Two kinds of tests were done: (1) IF loop-back; (2) satellite reception of signals from TDRS-F3.

In-lab IF loop-back

In this test, the 1024-chip PN sequence, with BPSK modulation at an IF of 72.003 MHz, was supplied to the SAW matched filter. This test confirmed proper PN sequence generation, matched filter operation, demodulation, frame synchronization and DAS operation. Through varying E_s/N_0 of the input signal, these subsystems were checked over the entire operating range. Figure 2.17 shows the output voltage at the envelope detector with a varying E_s/N_0 from 25 dB to 5 dB in one decibal steps. The time indices from 1 to 30 correspond to an input E_s/N_0 of 5 dB. The next group of 30 indices has a E_s/N_0 of 6 dB, and so on. Therefore, the last group of indices from 600 to 630 represents an input E_s/N_0 of 25 dB. It was seen that although there was a nonlinear relation between the input and the output (primarily due to the envelope detector), this relation was consistent as expected. The test also showed that this system functioned over a dynamic range of 20 dB which was almost identical to the theoretical range of 21.1 dB given in Table 1, accounting for there were some uncertainties in the link budget calculation.

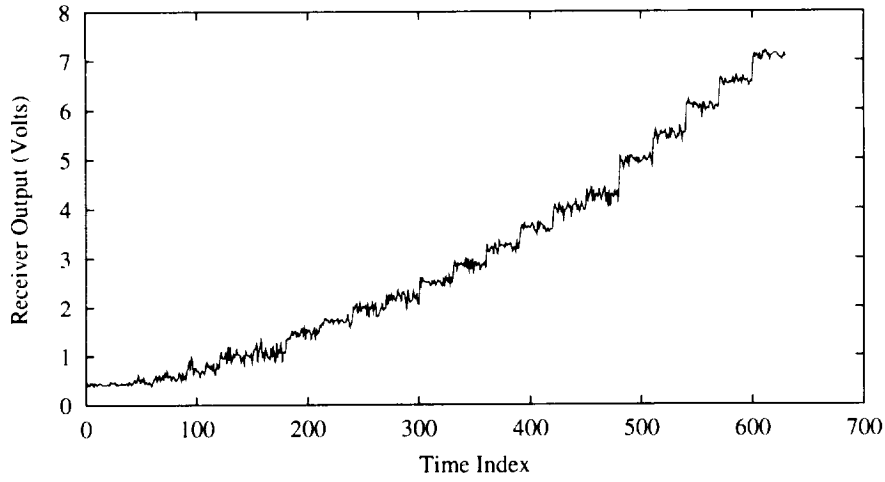

Figure 2.17 Voltage at Receiver Output during System Calibration

In-lab satellite reception

The in-lab reception of the PN sequence from TDRS-F3 tested all subsystems in the entire link from the transmitter to DAS. During the test, TDRS-F3 alternately transmitted the PN signal and carrier so that E_s/N_0 level could be analyzed. The entire range of E_s/N_0 was checked by varying the transmitted power of TDRS-F3. Figure 2.18 shows the actual E_s/N_0 vs the observed E_s/N_0 in dB. The actual E_s/N_0 was varied approximately 2 dB each step. The test data was indicated by the points and the curve fitting was represented by the solid line. This fitting curve of the 3rd order polynomials was used to compensate the nonlinearity of the measurement system in propagation data processing so that the actual signal strength level could be restored. Again, the input-output relationship was consistent and the test was a success.

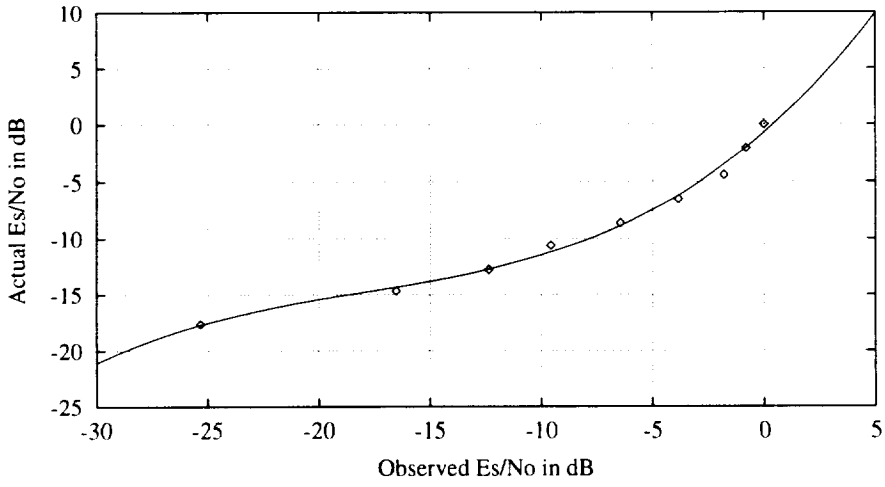

Figure 2.18 Measurement System Calibration Curve: Input vs Output

2.5 Conclusions

In this Chapter, the hardware and software systems design of S-band propagation measurement as well as system test and validation was detailed. The hardware system consisted of a ground-based transmitter, a mobile receiver, and a data acquisition system. The hardware system design and parameter selection were around the SAW match filter from Mobile Datacom Corporation, which matched a special 1024-bit-long PN sequence at IF of 72.003 MHz. By measuring and processing the output of the matched filter at baseband, the channel fading statistics can be analyzed. The software system was used in data acquisition and its design was based on the HP54505B digitizing oscilloscope, IEEE-488 interface and 486-PC. Descriptions of software usage and sample data collection process were also included to visualize how the measurement system was working in real environments.

To ensure the propagation data trustworthy and free of error, the measurement system (both hardware and software) was cross checked by two different approaches, i.e., the in-lab IF loop-back test and the in-lab satellite reception test, for the entire operating range. Through tests, the measurement system was checked for both proper operations and system performances, such as dynamic range, nonlinearity, minimum E_s/N_0, an so on. The nonlinear property was used to correct "raw" measurement data in calculation of Cumulative Distribution Function of the following chapters.

3. Data Collection and Fade Statistics

3.1 Introduction

This chapter will shift the focus from the details of the expirmental apparatus onto using it to collect propagation data. The goals of the measurement program were to observe channel fading in areas which were representative of cities, suburban areas, forests, tree-lined roads, mountains, and canyons. To achieve these goals, NMSU took the experiment out on two expiditions through the Western and Southeastern regions of the United States. The routes traversed took the experiment through many of the country's National Parks, where many textbook examples of a variety of topological and geological features are accessible by road. Along these routes, data was collected in major urban areas and along tree-lined interstate and secondary roads.

The chapter is divided into three main sections. First, an overview of the experimental concept is given, which will show how the components of the apparatus function together to measure fade statistics. Next, the details of how data was collected in each location are given. Finally, the fade statistics are presented, and some preliminary comparisons made. Complete records of the propagation data and fade statistics are contained in Appendix A, and detailed comparisons will be covered later in this report.

3.2 Experimental Overview

To accomplish the task of measuring channel fade statistics for a spread spectrum communications link, a spread signal was transmitted from orbit to an instrumented mobile receiver. For this research, the spread signal was uplinked at Ku-band through the White Sands Ground Terminal (WSGT), to TDRS F3, from which the signal was relayed back to the mobile receiver at S-Band. Figure 3.1 illustrates the basic concept of the measurement.

The performance of the channel was characterized by measuring the energy in the received waveform as the instrumentation was moved through the test areas. The receiver was calibrated against line-of-sight signal levels, such that it provided a measurement of the excess path loss due to shadowing and multipath effects. To achieve the goal of developing accurate empirical channel models for a *variety* of environments, it was important to pick appropriate locations in which to collect the data. These locations should be representative both in elevation angle to the satellite, and in topographical features. Using TDRS F3 at 61° W, the elevation angle contours to the satellite were as

shown in Figure 3.2 below. It can be seen that the elevation angles vary from about 55° in southern Florida, to about 8° in the Olympic Peninsula of Washington.

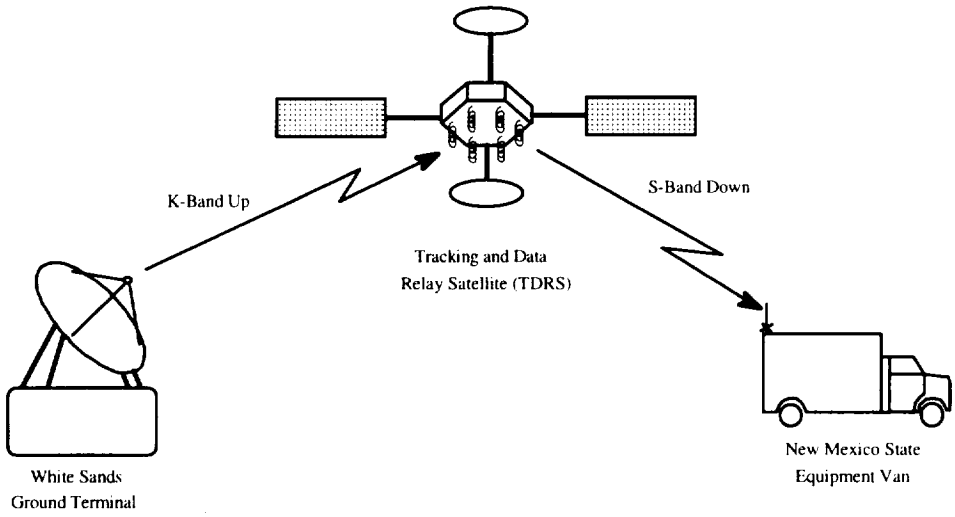

Figure 3.1 S-Band Test Concept

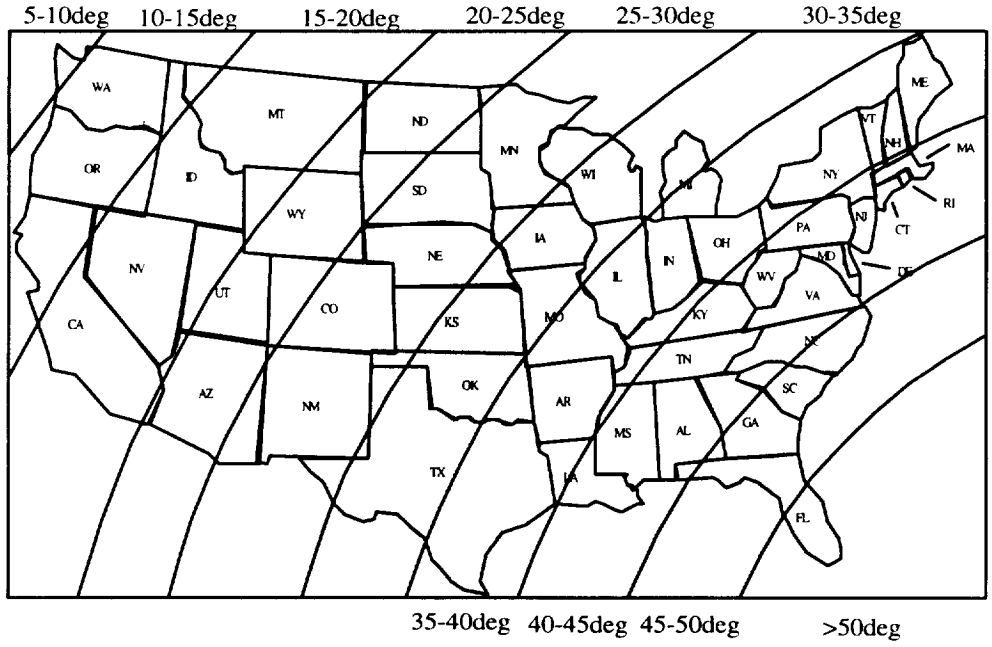

Figure 3.2 Look Angles to TDRS F3 at 61°W

The NMSU measurement system was designed around an analog SAW matched filter (refer to Chapter 2 for details). The filter was matched to a 1024-bit acquisition sequence derived from a much longer Gold code. The transmitter located at WSGT continuously transmitted this 1024-bit sequence as it was clocked out at an 8 MHz rate. The resulting BPSK signal, after filtering to the 3 dB points, occupied 8 MHz of bandwidth. After propagating through the channel, this signal was received, amplified, and downconverted for processing through the matched filter. At the output of the envelope detector, a waveform may be observed such as that depicted in Figure 3.3. There is a large response from the matched filter once per 1024 bit cycle. This response occurs when pattern of the incoming signal envelope is aligned with the geometry of the SAW device in the filter. The amplitude of the peak response is directly related to the total energy in the 1024 bit symbol.

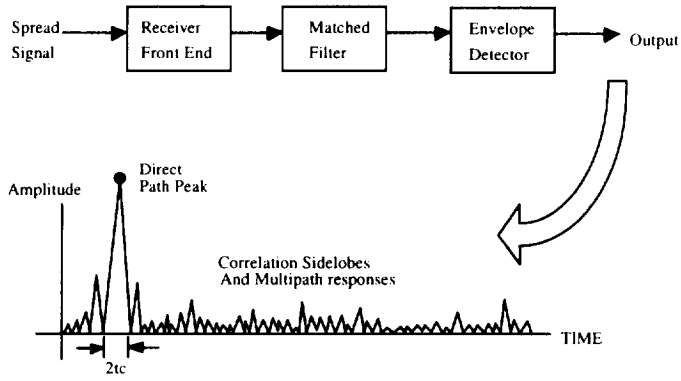

Figure 3.3 Response at receiver output

The principle of operation of this receiver structure is as follows. If there is no multipath present on the channel, there will be only one response at the output per 1024 bit sequence. If, however, multipath is present, it will appear as a time delayed and attenuated response at the output. Sampling the output of the matched filter provides a measurement of the delay profile for the channel for each sequence repetition, and the amplitude of the largest response in this profile provides statistics on the channel fading that would be observed by a single channel receiver.

The propagation data presented in this paper was collected by sampling the output of the matched filter at a 50 MHz rate. Sampling was not uniform since it was only desired to observe multipath returns from a few miles away. A special circuit synchronized the data collection to the transmitted sequence period, and samples were collected in 20 μs bursts around each peak response. Figure 3.4 shows the timing of the sampling. Each burst of data collection provides a measurement of the delay profile of

the channel, extending from -2 μs to +18 μs around the main response. With the hardware employed, it was possible to collect 30 delay profiles before pausing to download the samples to storage. The significance of this is that 30 delay profiles of the channel could be collected in rapid succession, but then a 3 second delay was required to store those profiles.

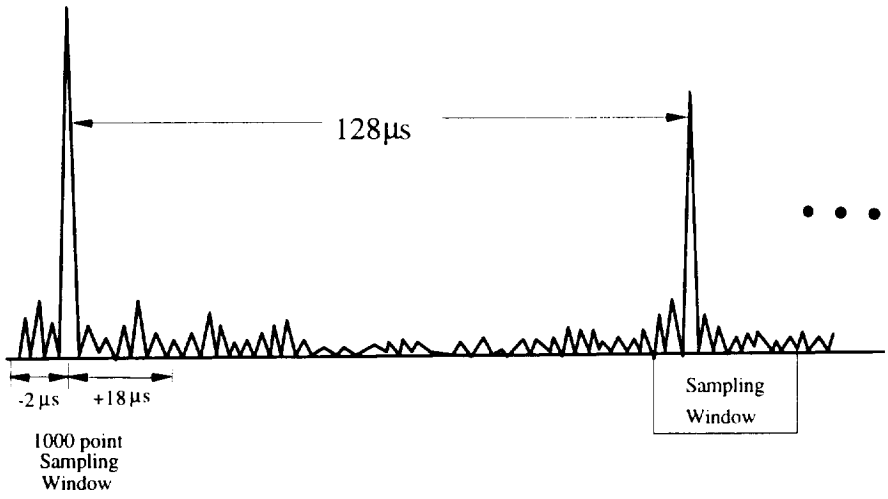

Figure 3.4 Timing of waveform sampling at the receiver output.

3.3 Data Collection

Data collection proceeded in two steps. First, the function of the system was verified with a satellite loop-back test, as detailed in the previous chapter. Following the equipment check-out and verification, propagation data was collected along two routes through the United States. The routes traveled were selected to provide measurement opportunity in a variety of environments. The first route, shown in Figure 3.5a, carried the experiment through the Western US, following a route north from Las Cruces, NM, to Denver, CO, to the Olympic Peninsula of Washington, to San Francisco, and back to Las Cruces. The second route, shown in Figure 3.5b below, encompassed much of the Gulf Coast region of the US, passing from Las Cruces to Houston, TX along I-10, up through Mississippi and Arkansas, then across the plains of Oklahoma and returning to Las Cruces.

In selecting the test areas, several propagation issues were kept in mind. In order to address questions about the performance of spread spectrum systems in multipath environments, it was necessary to collect data in areas where multipath was likely to occur. Because of the varying distances between sources of reflection in city environements and natural canyon/mountain areas, the multipath phenomena were

expected to have different characteristics. In response to these considerations, sites were selected in several major cities as well as in mountain and canyon areas. In order to compare spread measurements against models for CW fading along tree-shadowed routes, test areas in both heavy and light tree-shadowed environments were selected. Finally, several sites were selected in open areas, where fading was expected to be light. The resulting fade distributions were expected to be nearly identical (in a statistical sense) with similar distributions measured with CW experiments.

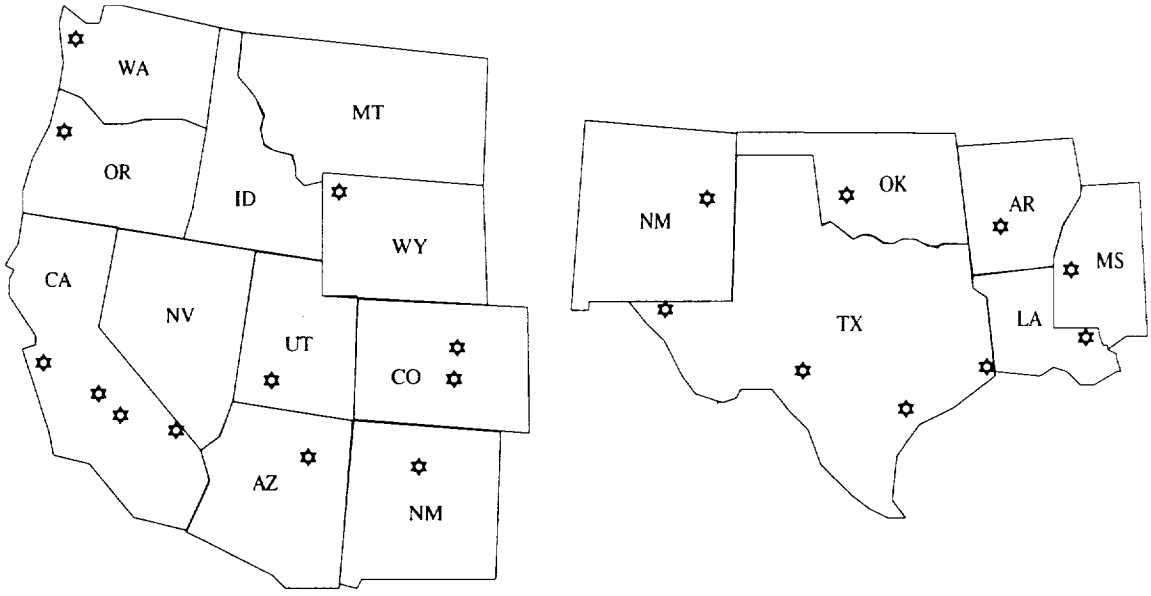

Figure 3.5 Details of the Routes along which Data Was Collected.
a) Western Route, and b) Southeastern Route.

In the two figures above, locations with a ✡ represent regions where propagation data was collected. The twelve locations along Route 1 included: Albuquerque, NM; Pikes Peak, CO; Denver, CO; Yellowstone National Park, WY; Olympic National Park, WA; Portland, OR; San Francisco, CA; Yosemite National Park, CA; Sequoia National Park, CA; Mojave Desert, CA; Zion National Park, UT; and US-180 through Arizona. Test areas along Route 2 included: I-10 from Anthony, NM to Kent, TX; I-10 from Sonora, TX to Seguin, TX; I-10 near Houston, TX; the Galveston, TX area; Central Louisiana, Central Mississippi, Central Arkansas, Central Oklahoma, and Eastern New Mexico.

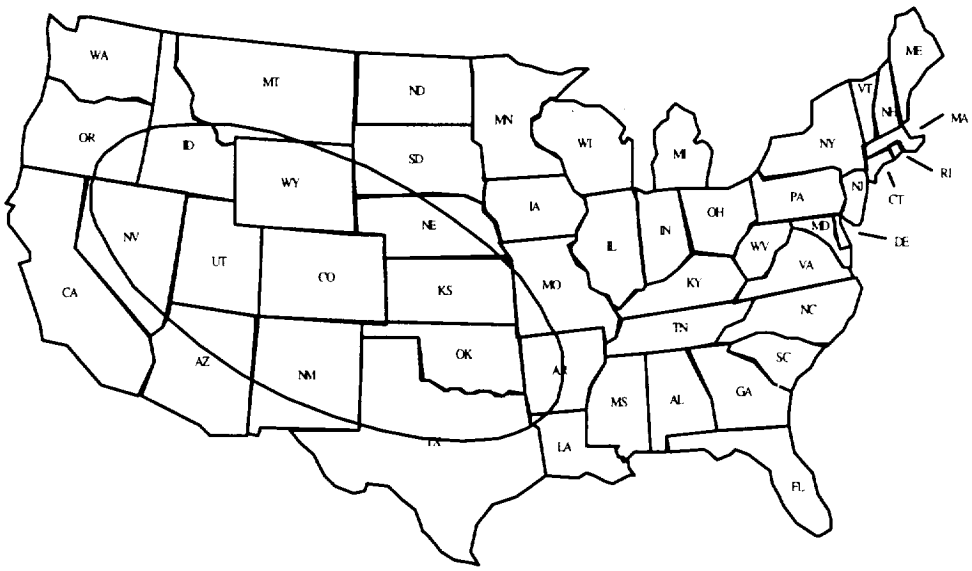

Figure 3.6 A Typical TDRSS S-Band 3 dB Footprint. Shown here with the Beam Centered on Denver, CO.

Figure 3.6 shows how the half power beamwidth of the TDRSS S-Band antenna compares with the size of the test areas. Under worse case conditions, where the receiver was moved at 65 mph during the three hours of data collection, the expected amplitude change due to movement through the antenna footprint would be less than 0.5 dB. In addition, the doppler observed on the signal due to the motion of the vehicle was on the order of 200 Hz, which also had no observable effect on the received signal strength.

3.4 Fade Distributions

Following the test plan summarized in the previous section, propagation data was collected in each of the locations specified. Approximately 100,000 individual delay profiles were measured at each location. To improve the effective signal-to-noise ratio, waveform averaging was employed. As described in Chapter 2, 30 delay profiles were collected within a few tens of milliseconds, at which time the data buffer was transferred to the PC. Each group of 30 delay profiles should represent essentially the same propagation environment, and by averaging these profiles, signal-to-noise performance was improved. The Cumulative Distribution Functions (CDF's) shown below represent the distribution of fades observed on the amplitude of the strongest return observable within each averaged delay profile. The fade depths are all referenced to unobstructed line-of-sight levels. Given the relatively small number of samples available for statistical analysis, probabilities less than .01 are not shown on the graphs.

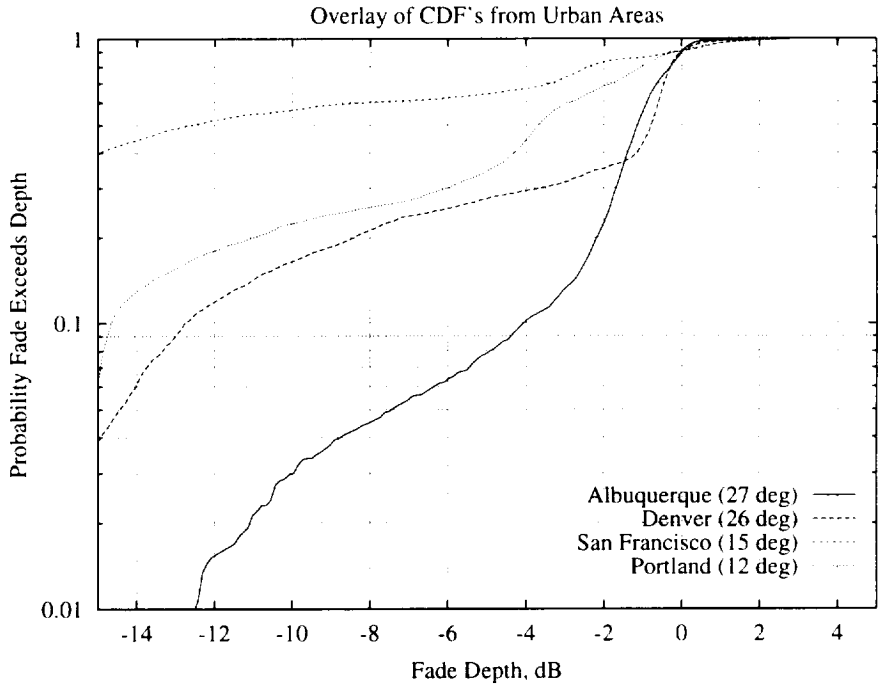

Figure 3.7 CDF's from Urban Areas

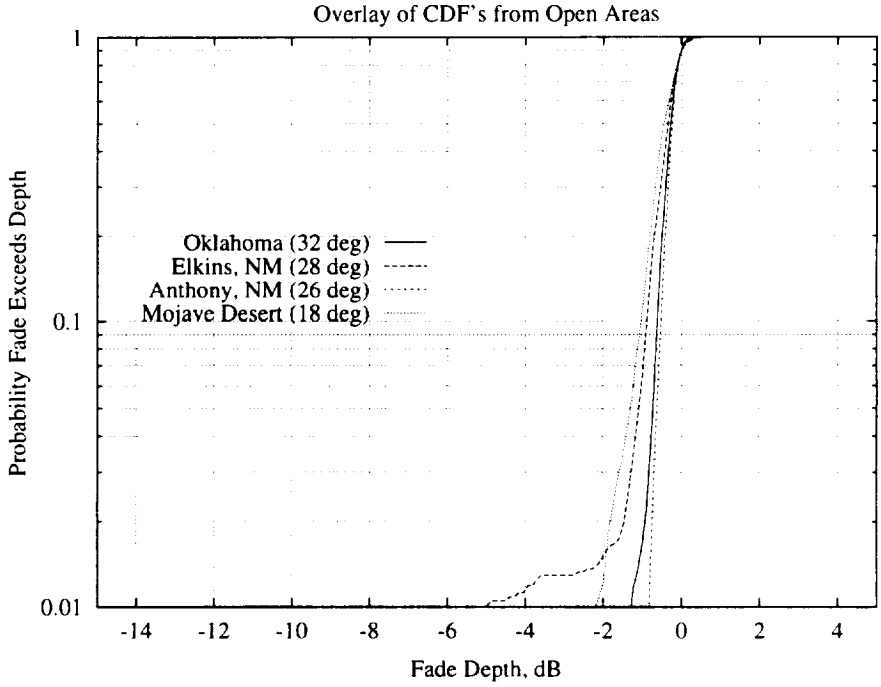

Figure 3.8 CDF's from Open Areas

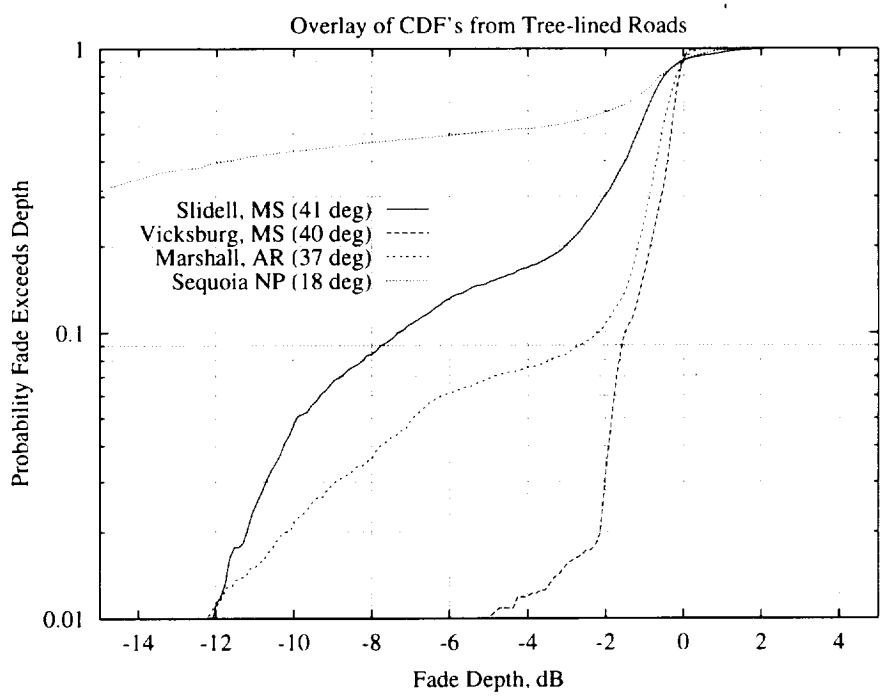

Figure 3.9 CDF's from Tree-lined Roads

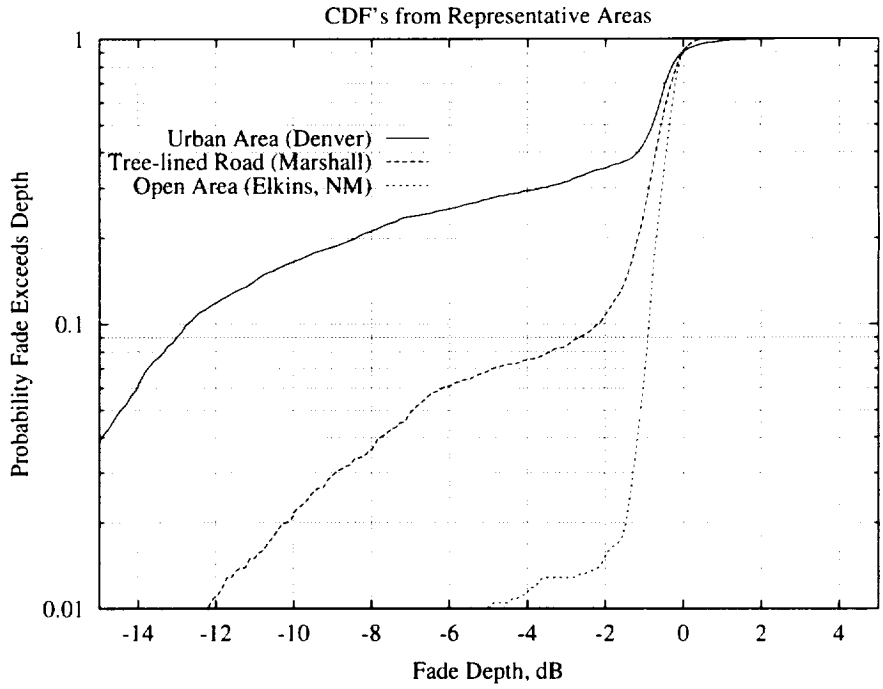

Figure 3.10 Overlay of the Curves from Three Representative Areas.

In Figure 3.7, several representative fade distribution curves are shown from urban areas. Figure 3.8 presents fade distributions for areas where unobstructed line-of-sight propagation was predominant. In Figure 3.9, the distributions from routes along shadowed roads are presented. Finally, Figure 3.10 shows an overlay of the fade distributions from figures 3.7 through 3.9. For a complete record of the individual data collected in each of the 21 areas, see Appendix A.

3.5 Discussion and Conclusions

In the previous section, the fade distributions observed by the S-Band receiver were presented. These curves exhibit two principle slopes. First, in the relatively open areas, the CDF's fall off very rapidly, with very low probability of deep fades. Those fades which do occur are primarily due to ground multipath and atmospheric effects. To see this, one may examine the geometry shown in Figure 3.11. The height of the mobile antenna is given as h, with the path elevation angle to the satellite given by θ . The differential path length is given as

$$\Delta = (R'+D) - R = R\left(\sqrt{1-4\frac{h^2}{R^2}\cos^2\theta} - 1\right) - \frac{2h\cos^2\theta}{\sin\theta} + \frac{2h}{\sin\theta} \cong 2h\sin\theta \qquad (3.1)$$

where the approximation holds as h/R goes to zero. This differential path length is less than $2h$ for all elevation angles, or 24 feet in the case of the NMSU experiment. The excess path delay is about 24 ns, which is much less than the 125 ns required for the spread system to separate the multipath.

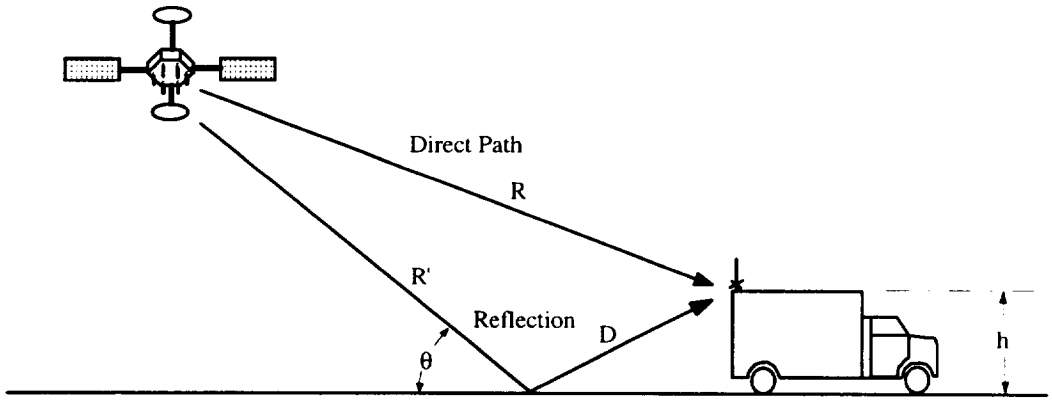

Figure 3.11 Multipath geometry on flat terrain.

In the heavily shadowed areas, the CDF's fall off very slowly, with high probability of deep fading. The open areas and shadowed areas comprise the two characteristic slopes for the CDF's. Test areas with a mixture of open and shadowed regions exhibit both slopes, with a knee separating the regions where each effect (shadowing and flat fading) is dominant.

Several statements may be made about the degree to which the fade statistics vary from one type of region to another. Refer to Figure 3.7, which shows the CDF's in several cities. At the .1 probability level, there is a 13 dB separation between the best and worst case fade depths exceeded (the worst case is actually off the graph). The curves are generally follow a pattern from low elevation angle to high, with the more severe fades occuring in the cities with lower elevation angles. However, it is seen that the fades in Portland, OR (12 degrees elevation angle) are not as severe as the fades in San Francisco (15 degrees elevation). This demonstrates that not only elevation angle but also the city itself determines the severity of the fading that will be observed.

Figure 3.8 does not hold many suprises. In the open areas, the fade distributions were strictly a fuction of elevation angle to the satellite. The best case fade distribution was measured in Oklahoma (where the highest elevation angle to the satellite was observed), while the worst case fade distribution was measured in the Mojave desert (where the lowest elevation angle to the satellite was observed).

Figure 3.9 shows a similar trend in the tree-shadowed environments to that of Figure 3.7. Generally, the lower the elevation angle to the satellite, the more severe the fades become. The data collected between Slidell, LA and Bolton, MS appears to have experienced deeper fades than elevation angle alone would account for. Again, the specific type of tree, size of the crown, and spacing between trees are all factors which impact the degree of fading observed.

The performance differences between heavy shadowing (urban), light shadowing (roadside trees), and open areas is clearly evident in Figure 3.10. The knees in the curves which separate the regions where flat fading and shadowing dominate are also evident. Flat fading is observed in all environments; however, the more severe the shadowing is, the sooner the shadowing effect dominates the fade distribution. In the open area, the knee occurs below the .01 probability level and is not observed in the distribution. With light to moderate shadowing, such as along tree-lined roads, the knee occurs at about the 0.1 probability level. Finally, in the urban environment, the knee has moved all the way up to the 0.3 level and dominates nearly the entire fade distribution curve. The best-case, worst-case, and median fade levels observed during the data collections are summarized in Table 3.1.

Geographic Area	Best-Case	Median	Worst-Case
Urban Areas	-4 dB	-10 dB	-17 dB
Tree-line Roads	-1.5 dB	-8 dB	-16 dB
Open Areas	-0.5 dB	-0.8 dB	-1.0 dB

Table 3.1 Summary of Fade Depths at the 0.1 Probability Level in Three Types of Environments.

4. Comparisons between CW and Spread Spectrum Fade Statistics

4.1 Introduction

In this chapter, we shall consider the relative performance of the communications channel for a spread spectrum signal and a CW signal. The basis for comparison will be the Cumulative Fade Distributions as measured for each type of system. It is hoped that these comparisons may answer some of the questions that have been raised during the ongoing debate between the proponents of spread spectrum systems and the traditional narrowband techniques. At the center of this debate is the fact that spread systems have an inherent ability to reject multipath whose relative time delay exceeds one chip period. This is demonstrated in Figure 4.1, where we see the nature of the spread spectrum receiver. This receiver will acquire the spread signal and synchronize with the spreading function. Bit decisions are made by sampling the peak response at the output of the matched filter. A basic property of the spreading functions is that the correlation is very small if the sequence is shifted by more than a chip time. Multipath components which have path delays in excess of a chip time do not affect the sampled peak amplitude. Thus, under many multipath situations the spread system should not see multipath fades that the unspread system would experience. If most multipath geometries found in the real communications channel have time delays greater than the chip duration, then the spread system would appear to be a better choice; however, no measurements have been published that compare the performance of spread systems and unspread systems on typical real channels.

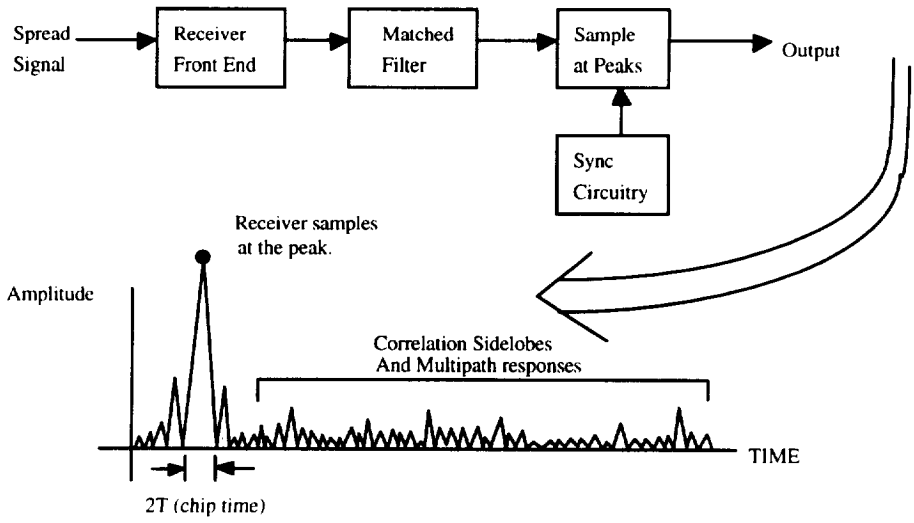

Figure 4.1 Processing of a Spread Spectrum Signal

The CW measurements that will be presented in this work have been taken from [4], [6], and [10]. In these experiments, a helicopter transmitted a beacon at 1500 MHz to a mobile receiver which navigated the terrain. The elevation angle was held to a tolerance of +/- 2° by manuevering the helicopter. Published CW data was available at elevation angles of 30°, 45°, and 60° [6] and [10]. In addition, some measurements were made using a satellite beacon on MARECS-B2, at an elevation angle of 21° [4]. The spread data was collected by NMSU as described in the previous chapters. In making the comparisons with the NMSU spread spectrum data, the terrain type and elevation angle most closely matching those of the NMSU data were selected. However, it should be noted that no *absolute* comparisons are possible without simultaneously collecting both CW and spread data along the same route at nearly the same times. Nonetheless, some general observations may be noted that provide some insight into the CW versus spread issue.

4.2 Calibration

In order to make comparisons between the data sets, it is important for them to be calibrated to the same reference level. In the NMSU experiment, every attempt was made to determine the absolute line-of-sight reference level, and then calibrate all observed fade levels to that reference. This resulted in CDF's with nearly 100% of the measured amplitudes falling below the 0 dB reference level. In contrast, the CW measurements used for comparison took a different approach to the calibration problem. If the Rician fading model is assumed to be valid, then theory predicts that 50% of the fades will be below the 0 dB level. That is, half the time the signals add constructively and produce an enhancement to the signal, while the other half of the time the signals cancel and cause fades. Using this information, the CDF's may be calibrated by adding a suitable constant to the amplitude data such that 50% of the fades exceed the 0 dB reference. In the plots that follow, the NMSU data has also been adjusted so that the curves match at the 50% level, as in the referenced CW data.

4.3 Open Plains Propagation

We begin with the case where the mobile system is operated in an open plain or prairie. Under these conditions, the only multipath is expected to be minor diffuse scattering from the surrounding plains. NMSU collected propagation data in two such environments. In the first, the receiving van was driven west along I-40 in central Oklahoma. The average elevation angle to the TDRSS satellite was about 33°. These conditions are nearly identical to the CW data shown in Figure 5 of [6], where the

elevation angle was 45° and the data was collected in the open prairie. The geometry is shown below in Figure 4.2. It is important to note that this geometry implies that the maximum path length difference between the direct path and the ground reflection is exactly 2h, where h is the antenna heigth above the ground. For a typical mobile user, this path difference is constrained to be less than 36 feet (maximum vehicle height on US interstate is 18 feet), which is much less than the distance required for multipath separation (about 125 feet for an 8 MHz chip rate). We would expect the spread and unspread systems to exhibit the same fading performance under these conditions.

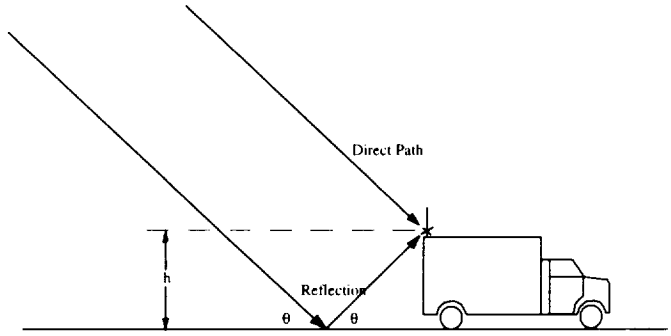

Figure 4.2 Geometry of Multipath in the Prairie

Figure 4.3 below shows the spread and CW curves overlaid. The most apparent feature of these curves is their similarity. There is no striking difference between these two curves. Upon close examination, one may observe a flat spot between the 50% and 90% levels on the CW data; this is due to the limited number of sample points that are available from Figure 5 of [6], and does not represent an event of any physical significance.

Figure 4.4 shows a second comparison between spread and CW propagation data. In this instance, the NMSU equipment was driven through the Mojave Desert in California. The elevation angle to the satellite was 18°, which is 12° lower than the corresponding CW measurement. Because of the large difference in elevation angles, the comparison is not expected to overlay as in Figure 4.3. Instead, it is expected that the fades will, on average, be slightly deeper for the lower elevation angle. The overall shape of the curve should, however, remain unchanged. As the figure reveals, the curves are indeed very similar, and the lower elevation angle results in deeper fades (by about 2 dB) at the 1% probability level. As with the Oklahoma prairie run, there appears to be no difference in the fade performance of the spread and the CW systems. While these preliminary comparisons are by no means conclusive, they do support the hypothesis that under open prarie driving conditions, spread spectrum modulation offers no improvement in channel fading performance.

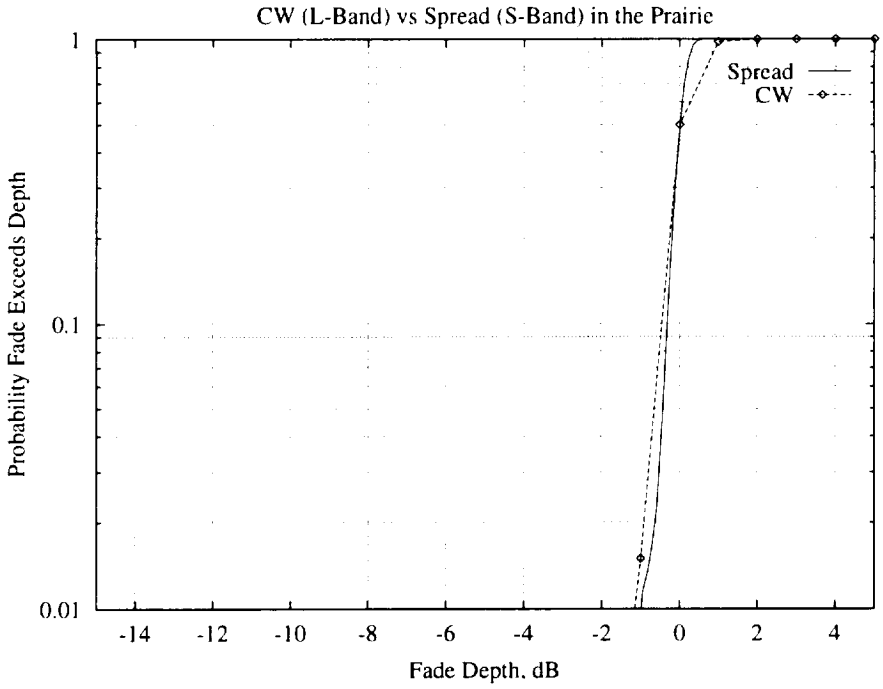

Figure 4.3 Spread signalling vs CW, in the Prairie

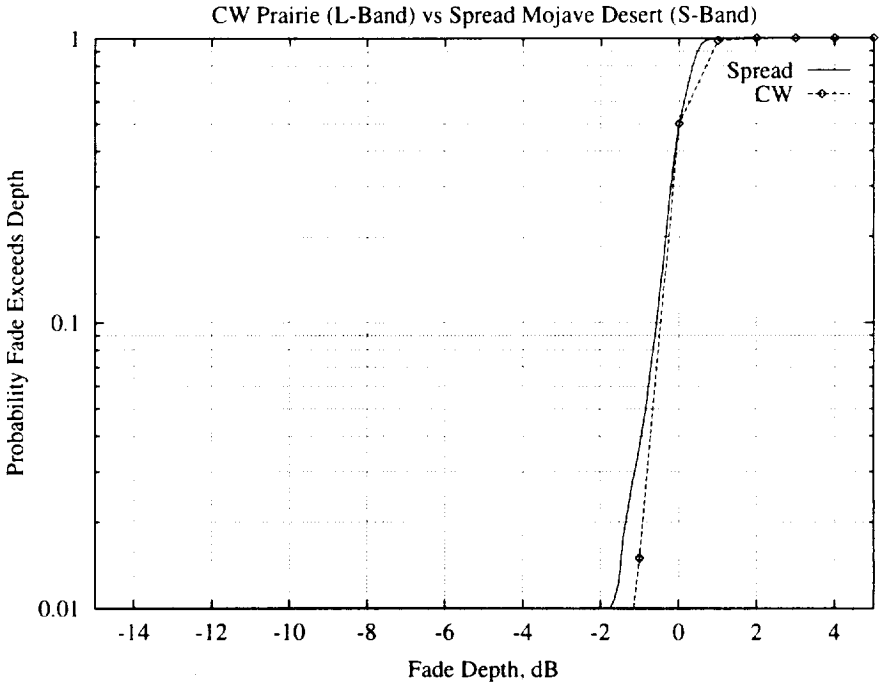

Figure 4.4 Spread signalling vs. CW, Mojave Desert, CA

4.4 City Canyon vs Natural Canyon

Multipath is expected to be at its worst in the city canyon environment. In this environment, the geometry lends itself to supporting single and multiple multipath reflections whose total path length difference may well exceed the minimum required for separation by the spread system. Because of the materials used in the construction of the buildings, these multipath signals are also likely to be large in amplitude. It is in this environment that the spread spectrum system has the most potential for system performance gains. Even so, by employing circular polarization in the system some of these effects may be mitigated. The first, and strongest multipath signal will become cross-polarized upon reflection. Thus it is the second reflection, of much weaker amplitude, that will most likely impact the system. NMSU collected data in several major urban areas, including Albuquerque, Denver, Portland, and San Francisco.

In order to get a first look at how the spread and CW systems might compare in the city canyon, it was necessary to find CW data taken under similar circumstances to some of the spread city data. The most similar CW reference data from those curves depicted in [4], [6], and [10] was collected in a natural canyon (Thompson Canyon), and is taken from Figure 7 of [6]. Natural canyons are not expected to produce multipath signals as strong as the reflection off of buildings. Also, the separation between the mobile transceiver and the sources of reflection may be much larger than in the city, where buildings are close together. The best comparison that can be made is between the Thompson Canyon data (30° elevation), and the Albuquerque data (27° elevation). Albuquerque was chosen both for the angle to the source as well as having the fewest buildings and hence the best approximation to a natural canyon.

Figure 4.5 shows the overlay of these data. The overall shape and character of the fading envelopes are very similar. While the Albuquerque data experienced deeper fades overall, this is consistant with the discussion above. No definite statement may be made regarding the performance improvement provided by the spread system, but it is clear that the spread system is subject to deep fades. The similarities in the curve shapes can also be used to argue that both systems are seeing the same types of fading phenomena, which is to say that the multipath fading is not separable by the spread system. A simple geometrical argument, such as that given in the previous section, can be used to show that the buildings must be *at least* 62 feet from the receiver to get separable multipath. This is on the order of the total width of most city streets, so it is possible that the dominant multipath is not separable by the spread spectrum receiver. Only multiple bounces, with the associated attenuation from each bounce, would give rise to excess path delays large enough to separate. This would tend to support the hypothesis that under typical city

canyon environments, an 8 MHz spread spectrum system is unable to reject the strongest multipath signal components, and experiences similar fade performance as unspread modulation systems.

4.5 Tree Shadowing Environment

Another case of interest is operation of mobile systems in tree shadowed environments. In these instances, the Rician fading model is not valid. This results in a slightly different calibration procedure for the data. The published CW measurements in the references have used a calibration level which results in 90% of all amplitude samples falling below the 0 dB fade level. For the purpose of comparison, the fade distribution functions from the spread measurements has been adjusted to also cross 0 dB at the 90% level.

Roadside tree shadowing is a problem across much of the eastern and southeastern regions of the United States. During the NMSU data collections along the Gulf Coast and the Mid West, several days worth of data was gathered along tree lined roads. Of these data collections, the data collected along the route from Marshall AR to Springdale, AR presented the best example of a typical tree lined road. The elevation angle to the satellite was a nominal 37° for the data collection.

The CW reference data was collected along MD 295, connecting Baltimore and Washington. The 30° elevation angle data was selected for comparison, as it most closely matches the 37° angle for the spread data. The tree cover along this route is similar to the Arkansas tree cover. The CW data was carefully collected in such a manner that roadside trees were present for the entire route. This resulted in a fade distribution without the knee which characterizes the change from multipath fading to shadowing. The spread data was collected in a less pure environement, and clearly shows the effects of both fading mechanisms. In the region from 1% to 20% fade probabilities

The conclusion that one arrives at upon examining Figure 4.6 is that the spread system does not appear to offer any performance gains over the CW system in a tree-shadowed environment. The model for tree shadowing accounts for fades through scattering and attenuation of the incident energy; there is no reason based in theory as to why the spread system would be immune to this type of fading. The data presented here support this view.

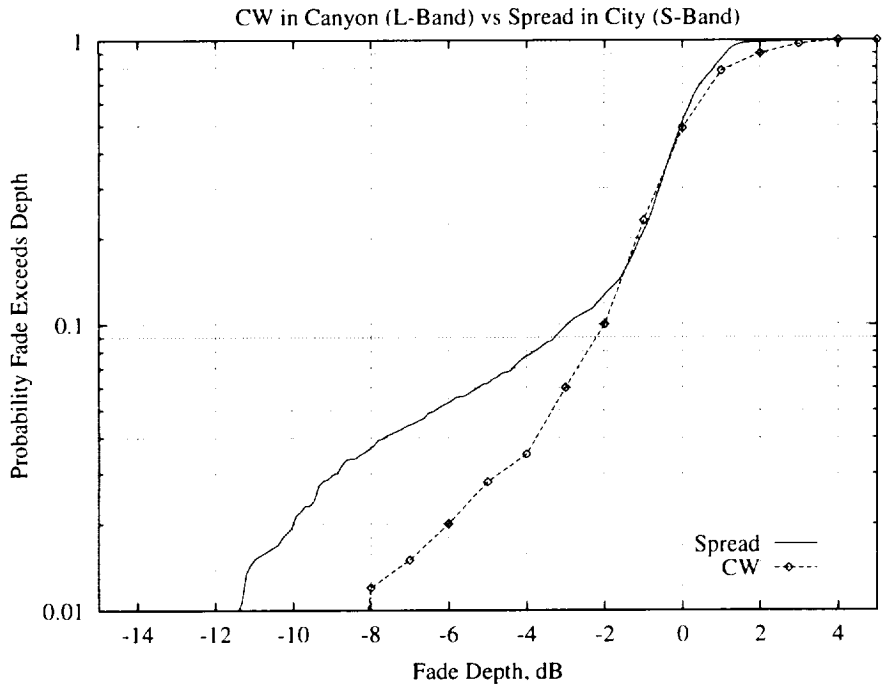

Figure 4.5 A Comparison of CW data in a Canyon with Spread data in Albuquerque

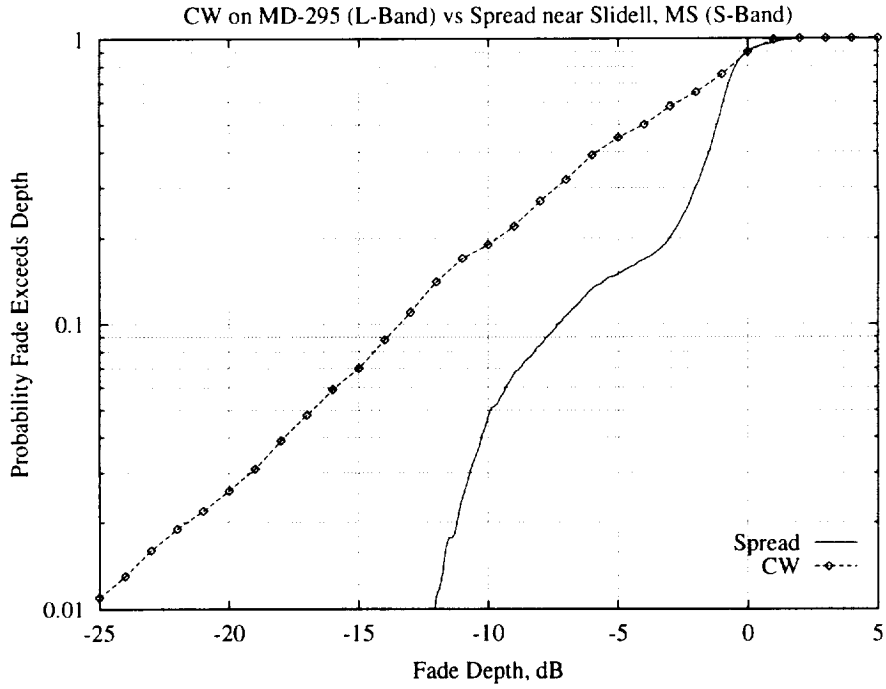

Figure 4.6 A comparison of CW data along MD 295 with Spread data along another tree-shadowed road at a similar elevation angle.

4.6 Conclusions

In the last three sections, fade statisctics have been examined in three types of environments. Comparisons between spread modulation systems and unspread systems in these environments have been made. For the case of propagation in open areas, it has been shown from geometrical considerations that multipath is not separable by an 8 MHz chip rate spread system. Measurements in open areas showed similar fade performance for both spread and unspread modulation, which supports the belief that spread systems will perform the same as unspread systems in the presence of unseparable multipath.

For propagation through trees along the roadside, the dominant fade mechanisms are hypothesized to be attenuation in the tree foliage in combination with some amount of unseparable multipath from the ground (as in the open areas). Comparison of spread and unspread systems in such roadside tree environments do not agree as closely as in the open areas, but the differences observed can be accounted for by differences in the degree of tree cover in the two areas compared.

The remaining area of interest is the city canyon, or urban area. In this environment, strong multipath induced by the large concrete and steel structures is expected to be present. Unlike the geometry of the open prairie, the urban geometry may support multipath with differential path lengths in excess of what is required to be separable. Thus, the theory would allow for some rejection of multipath induced fades in such an area. In examining the limited data available however, no clear evidence of such an improvement in the fade statistics is discernable. One possible explanation for this is that in practical situations, multipath is either too close to be separable, or too far away to have sufficient amplitude to cause deep fades.

These few preliminary comparisons are not inconsistant with the hypothesis that under the majority of mobile conditions likely to be encountered, spread modulation does not offer performance enhancement with respect to channel fading. In practice, we found no evidence of improvement in the few comparisons we were able to make in the city canyon environment using an 8 MHz chip rate spread system.

It is interesting to examine how the fade statistics derived from the spread measurements compare with models derived from CW measurements. Using the Empirical Roadside Shadowing Model described in [7], the fade statistics for a mobile system operating in a roadside tree environment at 37° elevation angle were computed. In Figure 4.7, this curve has been overlaid with the fade statistics from the spread measurements in central Arkansas. The spread measurement clearly shows the presence of two types of fading - multipath and shadowing. The knee in the curve marks the transition between the two. The slope of the shadowing portion of the CDF is identical

with that of the ERS model, but is shifted to the right. This shift to the right is accounted for because roadside tree shadowing was not present for the entire duration of the data collection.

The knee occurs at a fade depth of between 2 and 3 dB. If the portion of the CDF of interest is extrapolated, and shifted to correct for the time in which no roadside trees were present, then a fit such as that shown in Figure 4.8 results. The agreement between ERS model and spread measurement is good. This result indicates that spread systems exhibit the same degree of fading in tree shadowed environments as do unspread modulation systems.

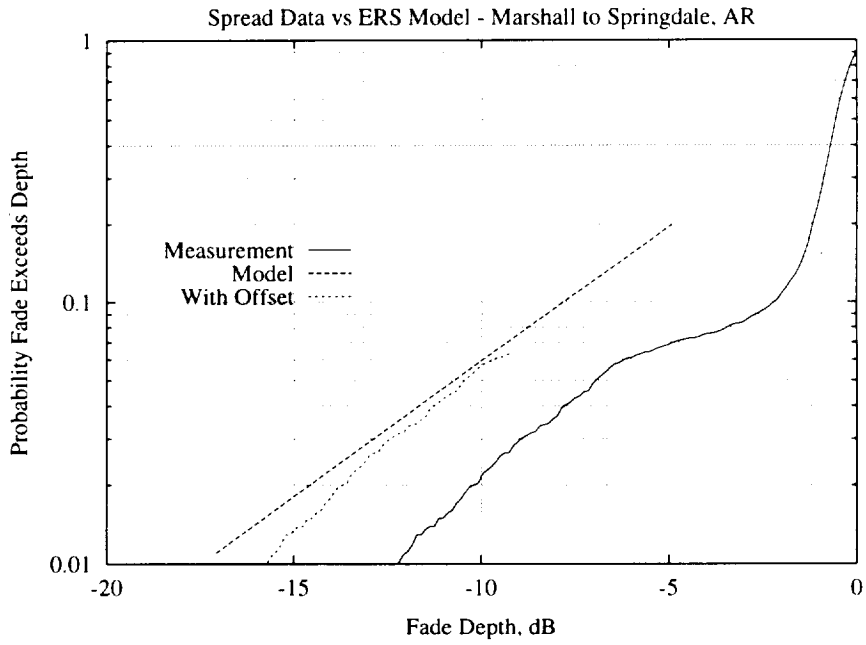

Figure 4.7 A comparison between the Empirical Roadside Shadowing model and the observed fade distribution at 37° elevation angle.

Some insight is gained by comparing measurements against models. However, to actually determine the improvement offered by spread signalling in typical operating conditions, it is necessary to collect simultaneous fade statistics for a spread signal and a CW beacon. Such information will allow the system engineer to deterimine if there are sufficient gains available from employing spread spectrum signalling to justify building such a system for a given operational area. An experiment to simultaneously measure the performance of spread and narrowband systems in the same environments is suggestested as the next step in studying the mobile communications channel.

5. Summary

The experiment reported in this document is an important beginning to understanding the effects of the mobile propagation environment on spread spectrum systems. What has been learned from these measurements, and what should be studied next?

Fade distributions have been collected in many environments of interest throughout the United States, and these curves may be used as a guide in determining required fade margins for spread systems.

In Chapter 2, the spread measurement system was described in detail. The accuracy and calibration of the system was validated through a series of measurements in the lab and through TDRSS. As a result of these tests, there is confidence that the measurement technique results in accurate measurement of fades on the spread communications channel.

In Chapter 3, the spread propagation data was presented. In examining the fade distributions, it was noted that elevation angle to the satellite has a large impact on the severity of fading on the channel. However, the specific environment also plays a significant role in the degree of fading. This makes it difficult to develop a model for propagation that applies to an average city, or an average tree-lined road, because of the physical differences between two locations. In the fade distribution curves, two regions can be discerned which correspond to multipath fading and shadowing. The presence of a knee in the curves between these two regions is evidence that in most environments, fading is caused by a combination of these two phenomena.

Several questions remain unanswered by this research. In particular, insufficient data is available for comparing the statistics of the fades seen by the spread system with those seen by a system using an unspread modulation scheme. In Chapter 4, some comparisons were made with the data that is available, but these are far from conclusive. Based on these limited comparisons, there is no evidence that spread systems are effective at rejecting multipath fades in the typical operating environment. To make such comparisons with any validity, spread and unspread fade measurements should be performed at the same time and place, so that all other environmental factors may be removed from the experiment. Under such circumstances, even slight performance differences may be attributed to the modulation scheme rather than experimental uncertainty. Such an experiment is proposed as the next logical step to understanding propagation for spread systems in multipath environments.

References

[1] Goldhirsh, J. and W. Vogel, "Propagation effects for land mobile satellite systems; overview of experimental and modeling results", NASA Reference Publication 1274, February 1992

[2] Vogel, W. and J. Goldhirsh, "Tree attenuation at 869 MHz derived from remotely piloted aircraft measurements", *IEEE Trans. Antennas Propagat.*, vol. AP-34, no. 12, pp. 1460-1464, Dec. 1986

[3] Goldhirsh, J. and W. Vogel, "Roadside tree attenuation measurements at UHF for land-mobile satellite systems", *IEEE Trans. Antennas Propagat.*, vol. AP-35, no. 5, pp. 589-596, May 1987

[4] Goldhirsh, J. and W. Vogel, "Mobile satellite system propagation measurements at L-Band using MARECS-B2", *IEEE Trans. Antennas Propagat.*, vol. AP-38, no. 2, pp. 259-264, Feb. 1990

[5] Vogel, W. and Y. Hase, "Land-Mobile-Satellite fade measurements in Australia", *AIAA Journal of Spacecraft and Rockets*, July-August 1991

[6] Vogel, W. and J. Goldhirsh, "Fade measurements at L-Band and UHF in mountainous terrain for land mobile satellite systems", *IEEE Trans. Antennas Propagat.*, vol. AP-36, no. 1, pp. 104-113, Jan. 1988

[7] Proceedings of the Eighteenth NASA Propagation Experimenters Meeting (NAPEX XVIII), JPL Publication 94-19, August 1, 1994

[8] Ghassemzadeh, S. et al, "On the statistics of multipath fading using a direct sequence CDMA signal at 2 GHz, in microcellular and indoor environment", *International Journal of Wireless Information Networks*, vol 1. no 2, 1994

[9] Ikegami, T. et al, "Field tests of a spread spectrum land mobile satellite communication system", *IEICE Trans. Commun*, vol. E76B, no. 8, August 1993

[10] Goldhirsh, J. and W. Vogel, "Mobile satellite system fade statistics for shadowing and multipath from roadside trees at UHF and L-Band", *IEEE Trans. Antenna Propagat.*, vol. AP-37, no. 4, pp. 489-498, April 1989

Acknowledgment

The authors wish to acknowledge the support of NASA under grant NAG-5-2141 for funding this research and making the TDRSS resources available for the measurements. We also wish to express our appreciation to Steve Kelly for his efforts in fabrication and installation of the hardware into the NMSU Engineering Dept. Van, to Al Carrier, Abe Valdez, Ted Wolcott, and Bill Drozdick for their efforts in fabrication and testing of the instrumentation, and to Bill Linde for his support with software and preliminary data reduction.

Appendix A

This Appendix contains the processed data from all 21 locations in which data was collected. Each page consists of the fade measurement vs. time, with the matching Cumulative Distribution Function below. all of these CDF's have had some small (typically less than 0.5 dB) offsets added so that the 90% probability level crosses at the 0 dB fade level. This is to make it easier to compare the curves with each other, as well as make comparisons with other curves appearing in the literature.

Albuquerque, NM

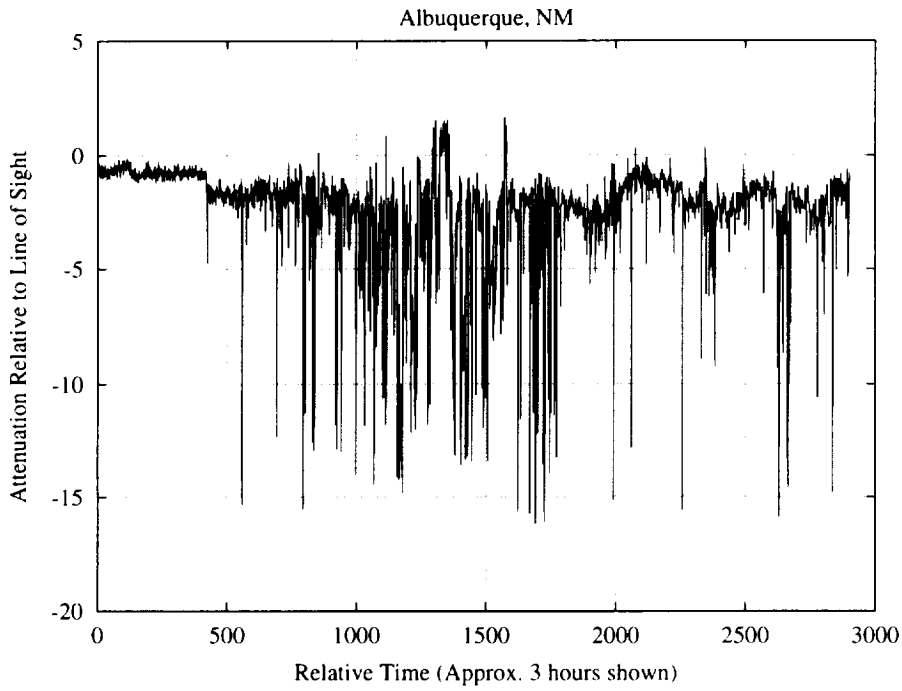

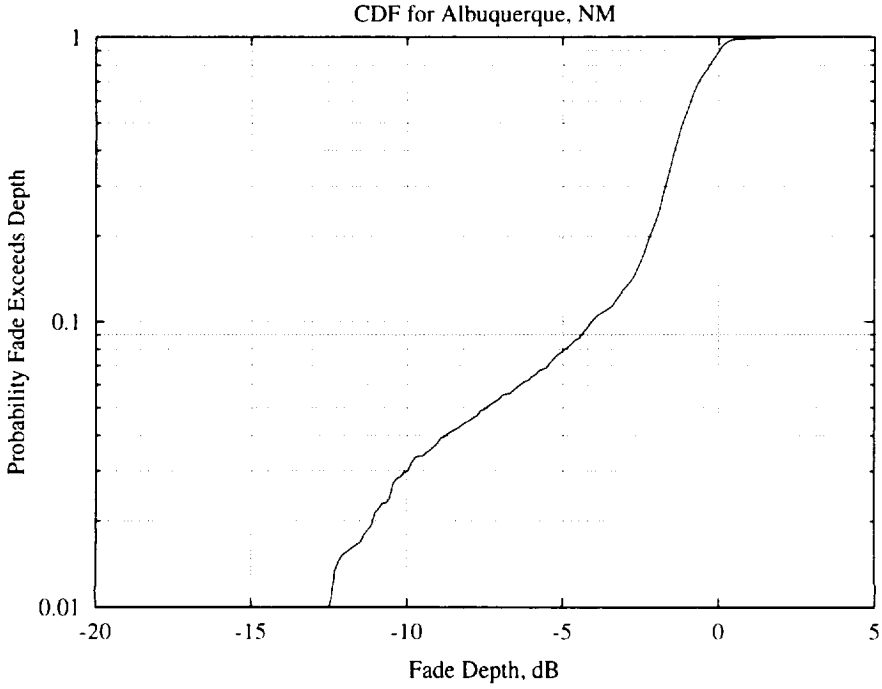

Anthony, NM to Kent, TX on I-10

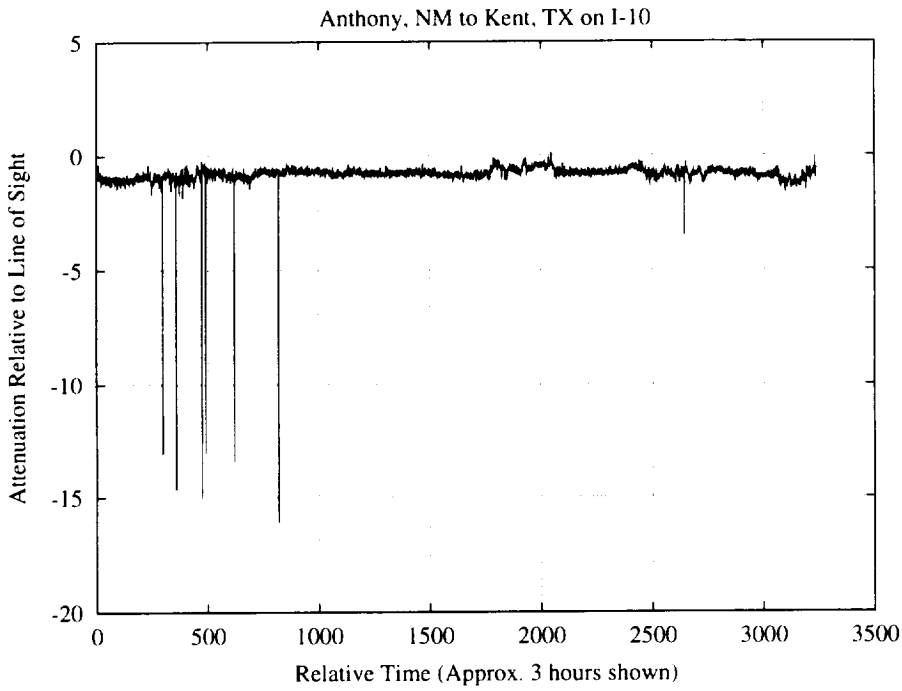

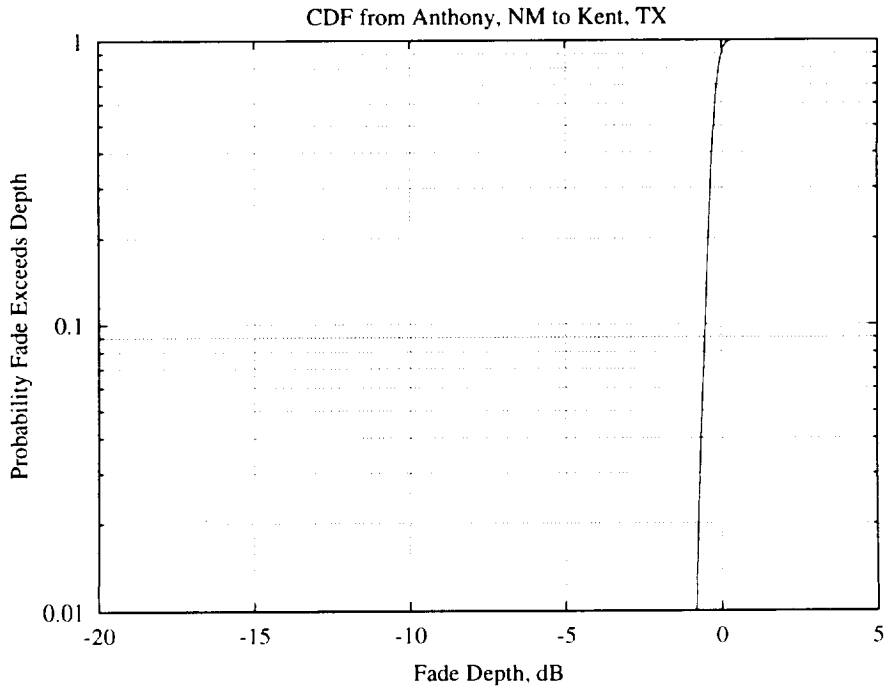

Bolivar, Tx to Port Arthur, TX

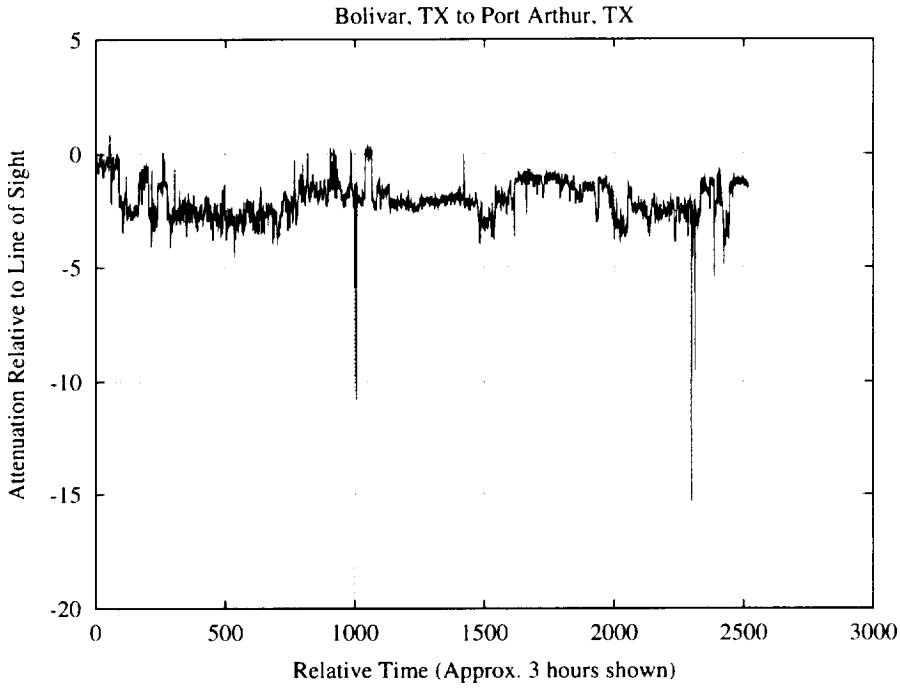

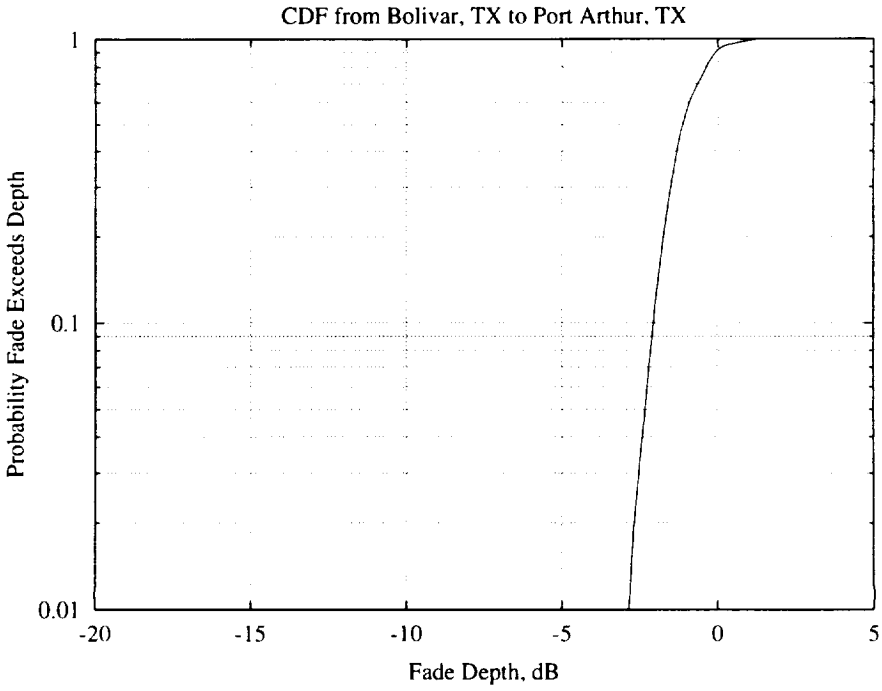

Denver, CO

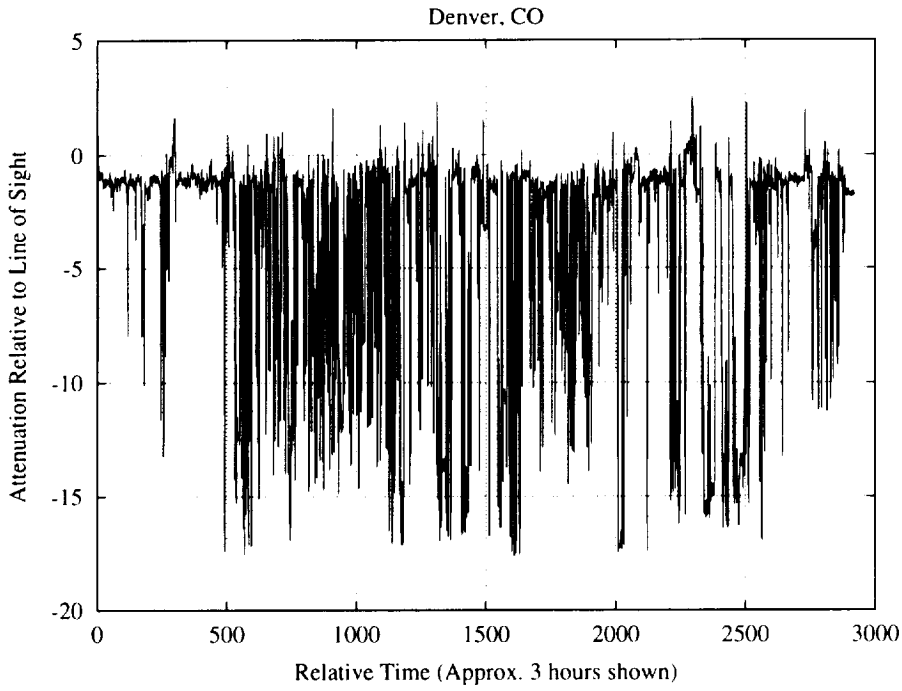
Denver, CO
Attenuation Relative to Line of Sight
5
0
-5
-10
-15
-20
0
500
1000
1500
2000
2500
3000
Relative Time (Approx. 3 hours shown)

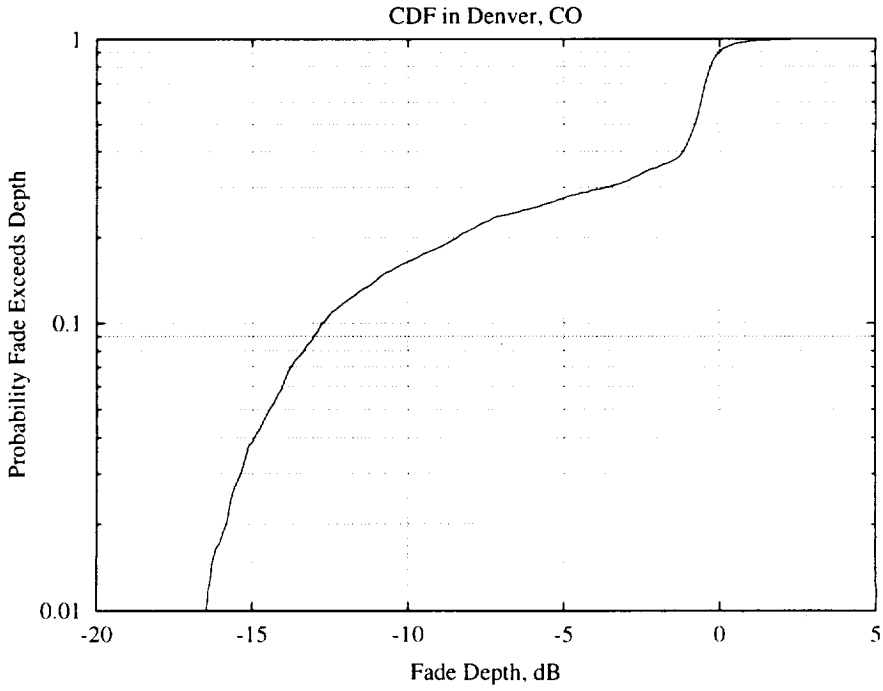
CDF in Denver, CO
Probability Fade Exceeds Depth
1
0.1
0.01
-20
-15
-10
-5
0
5
Fade Depth, dB

Elkins, NM to Alamogordo, NM

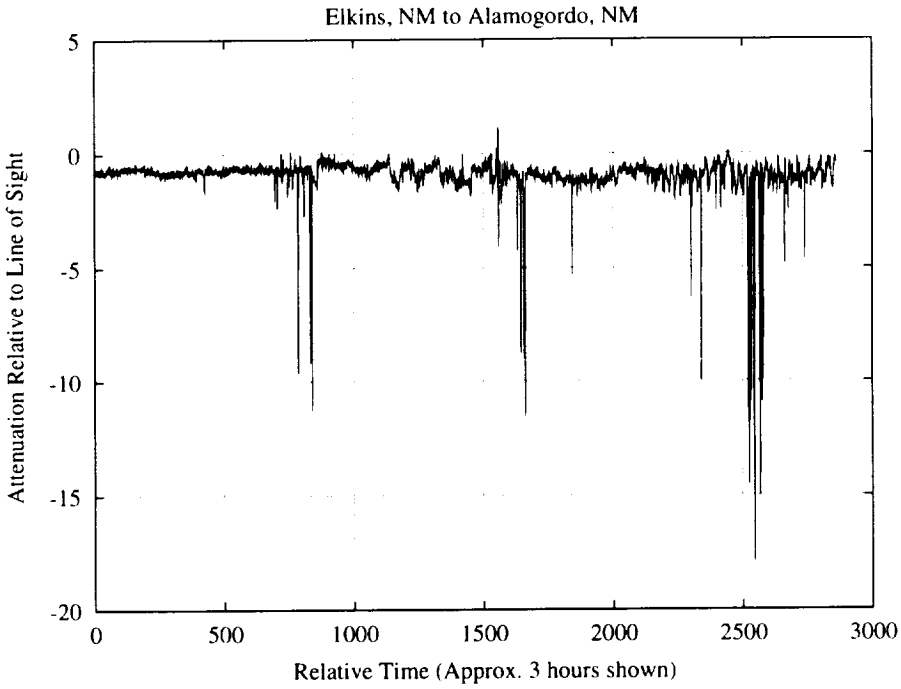

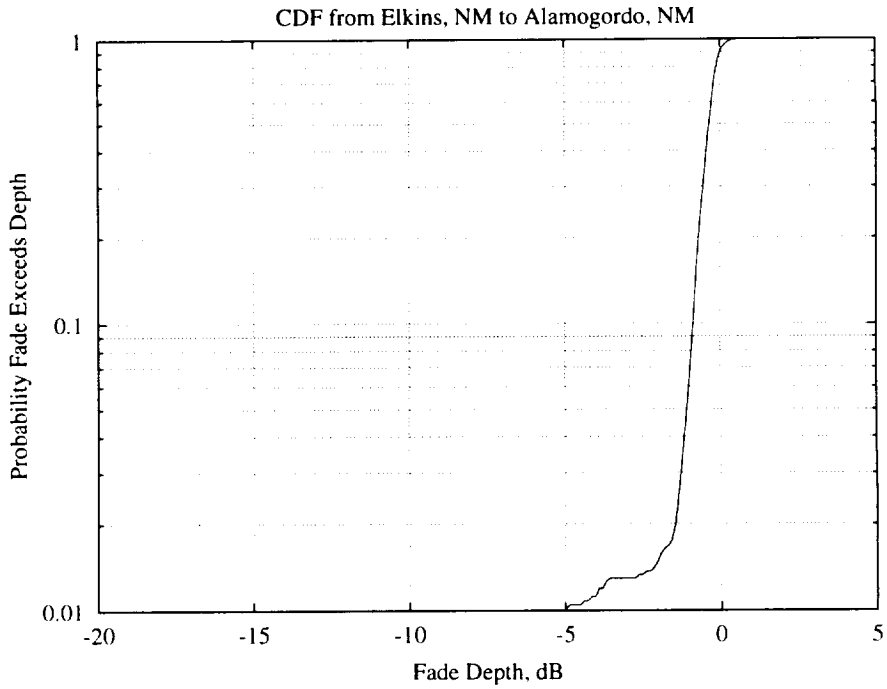

Katy, TX to Galveston, TX

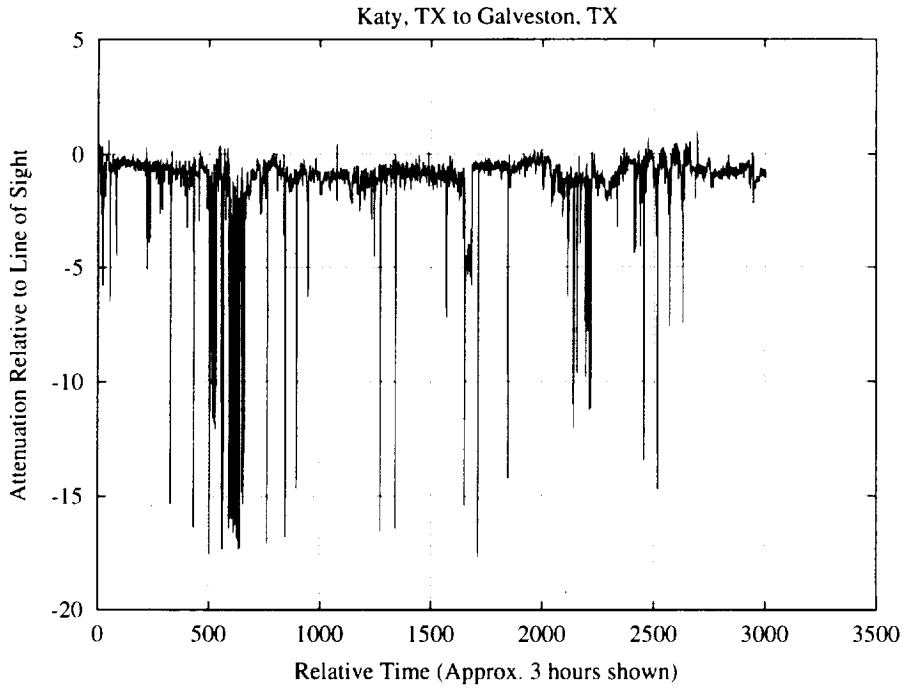

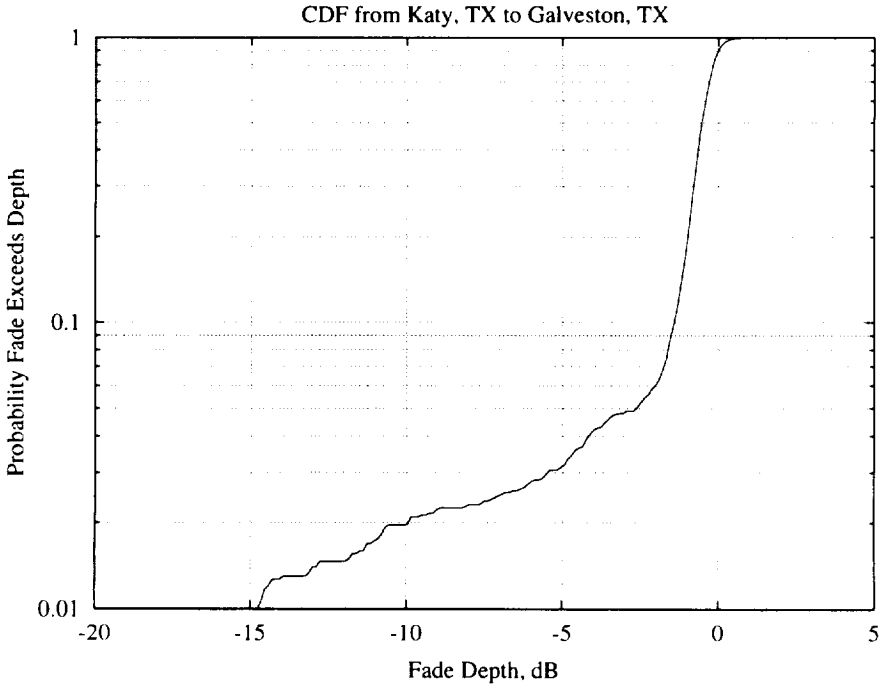

Marshall, AR to Springdale, AR

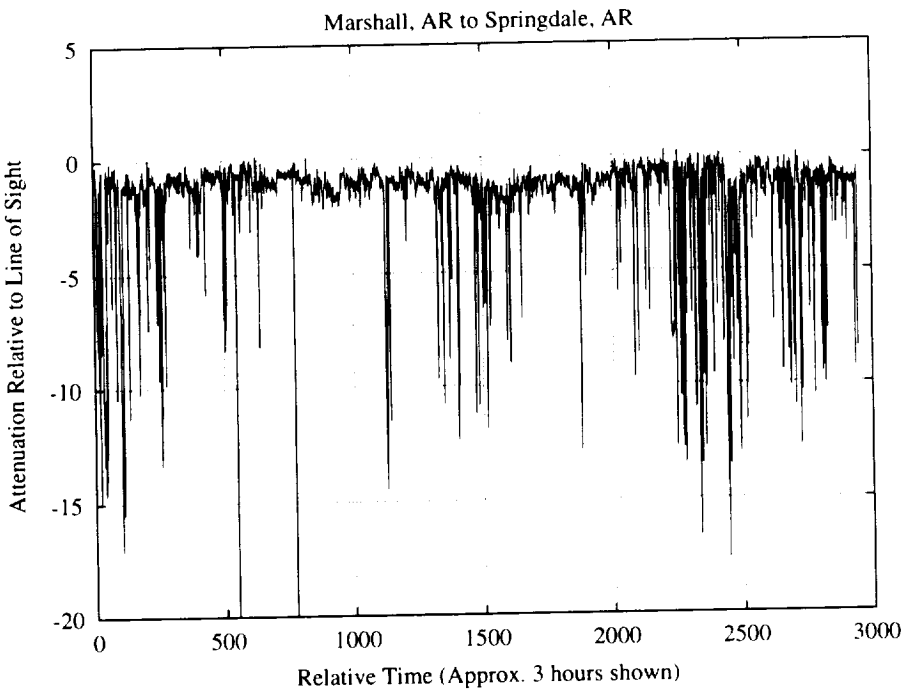

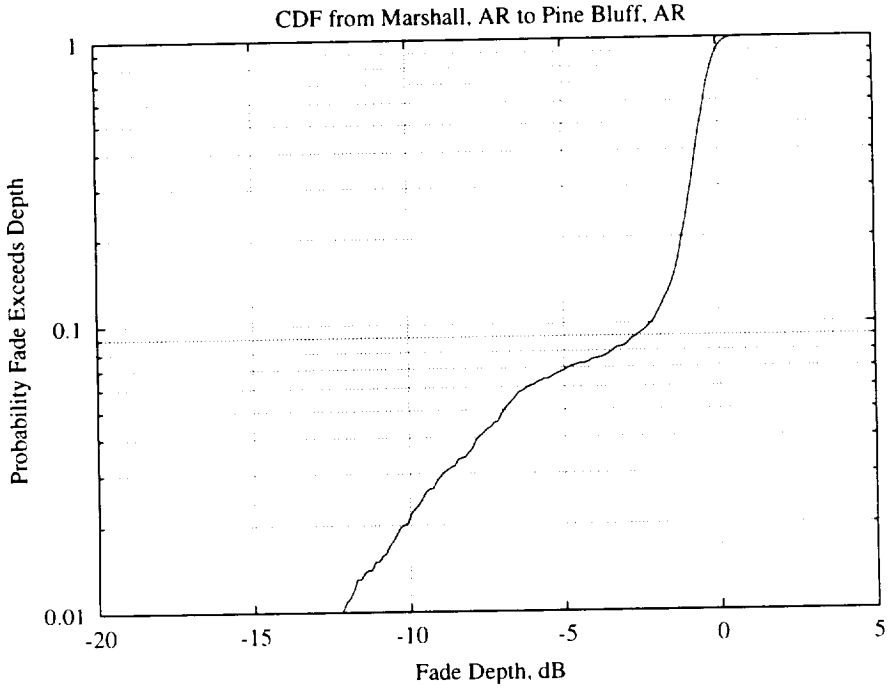

Mojave Desert, CA

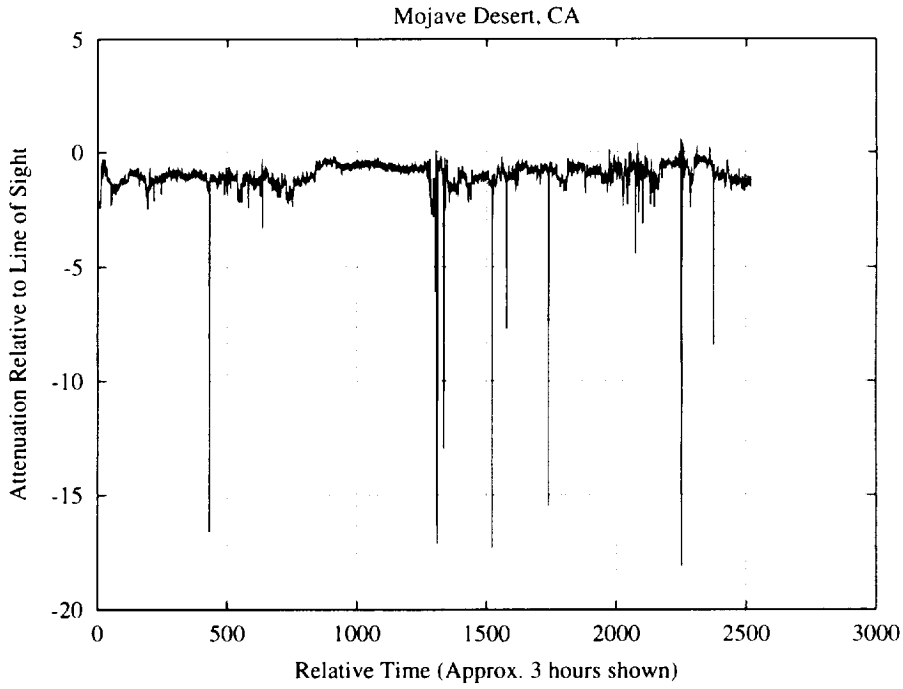

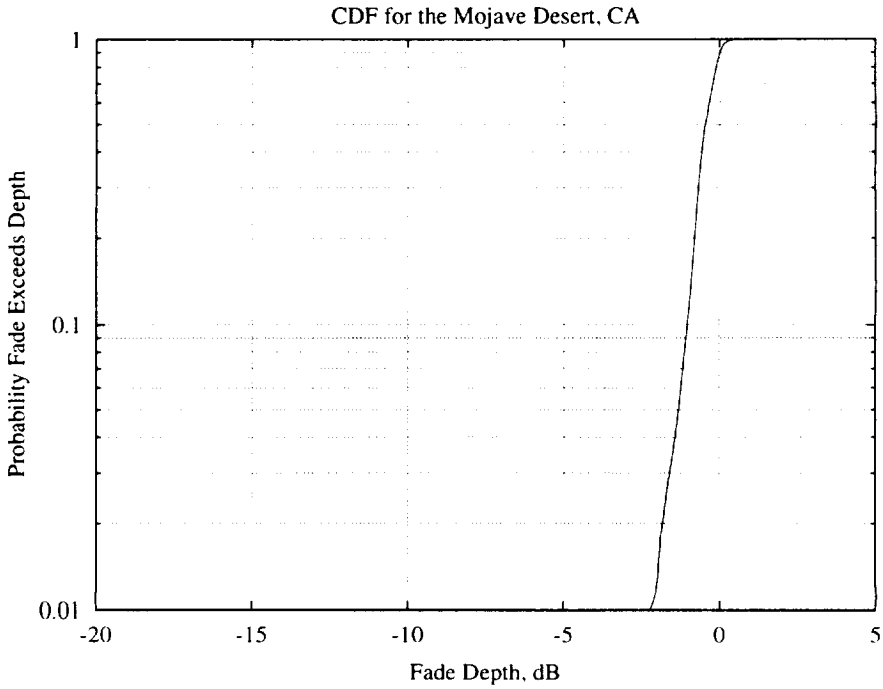

Oklahoma City to Elks, OK on I-40

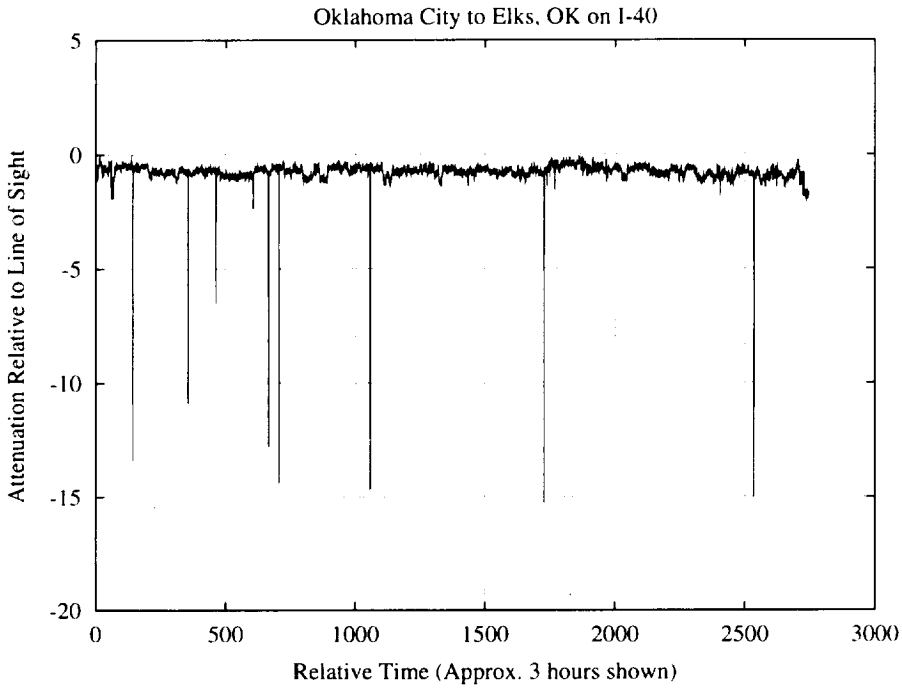

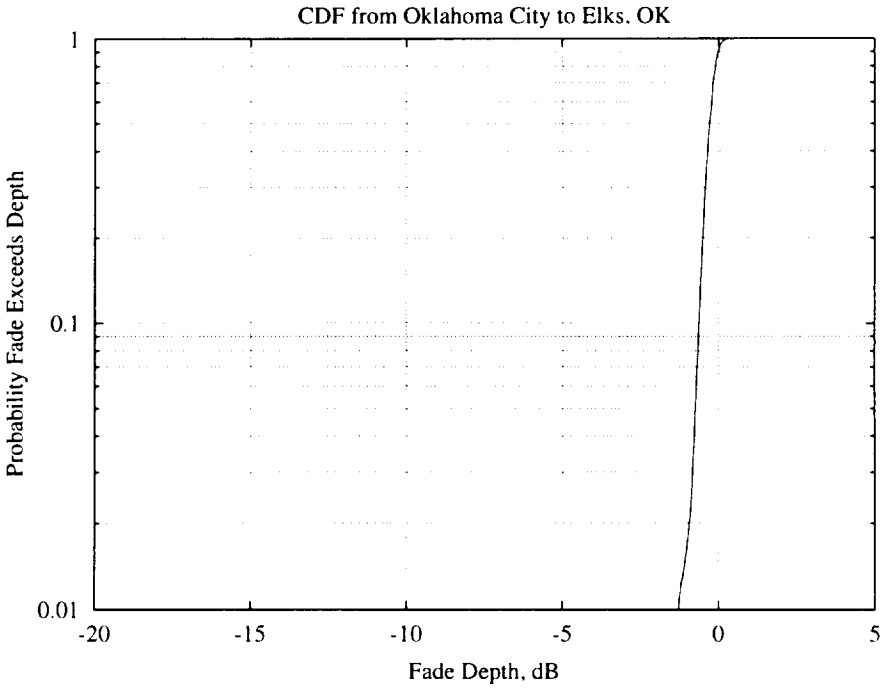

Olympic Penninsula of Washington

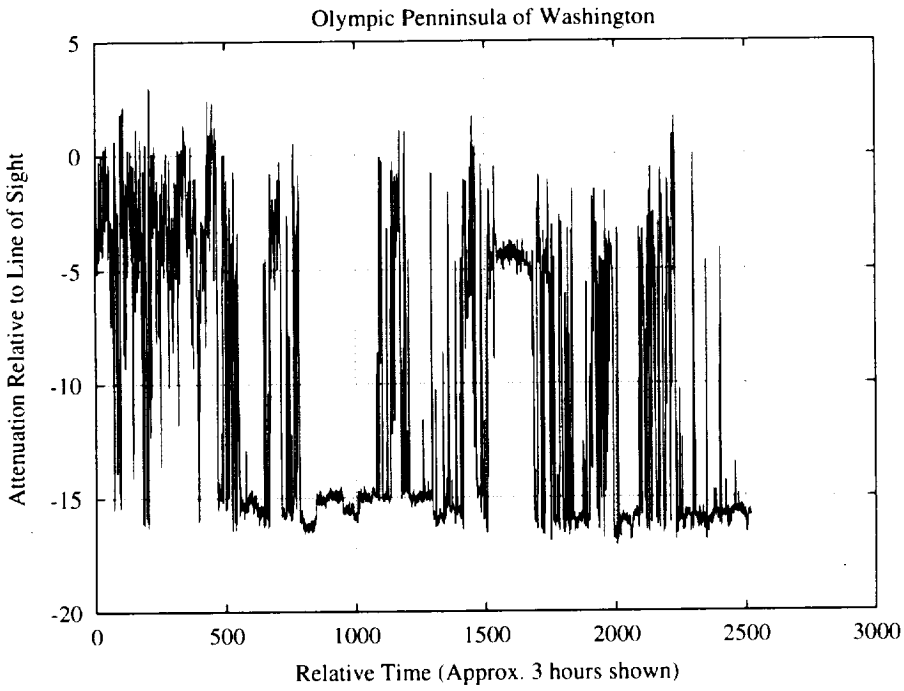

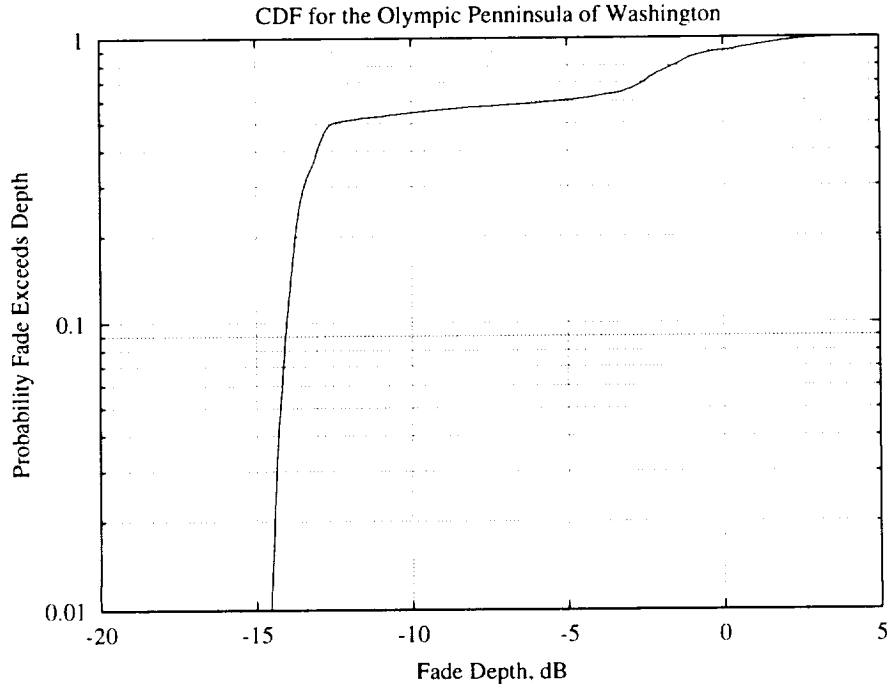

Pikes Peak area of Colorado

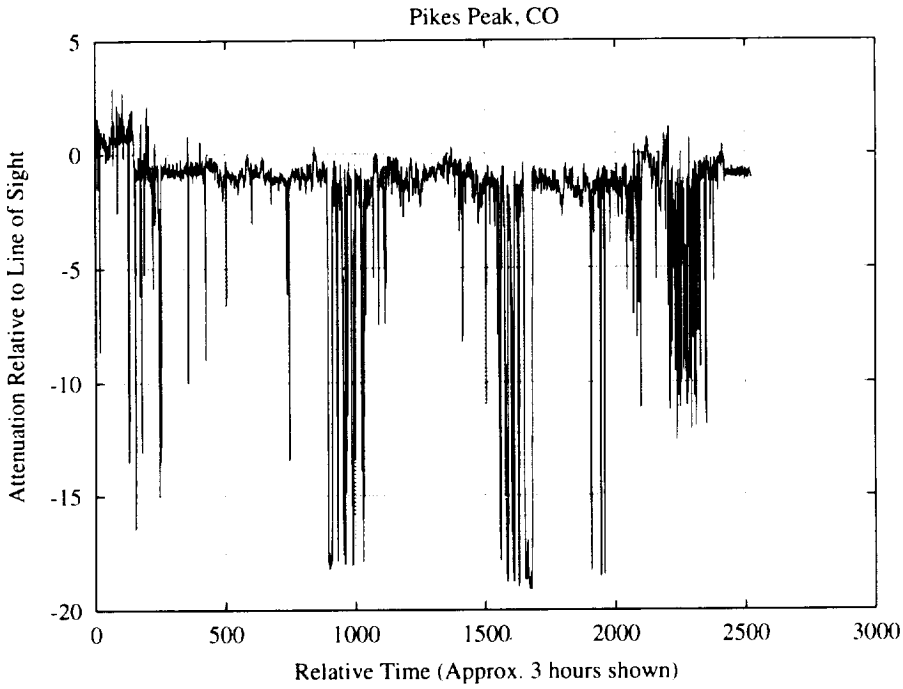

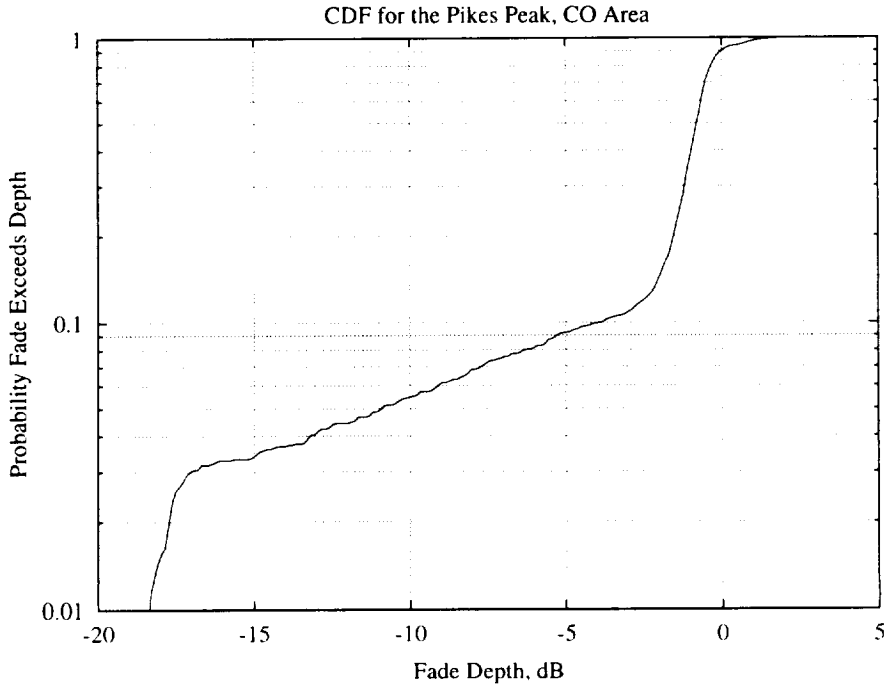

Portland, OR

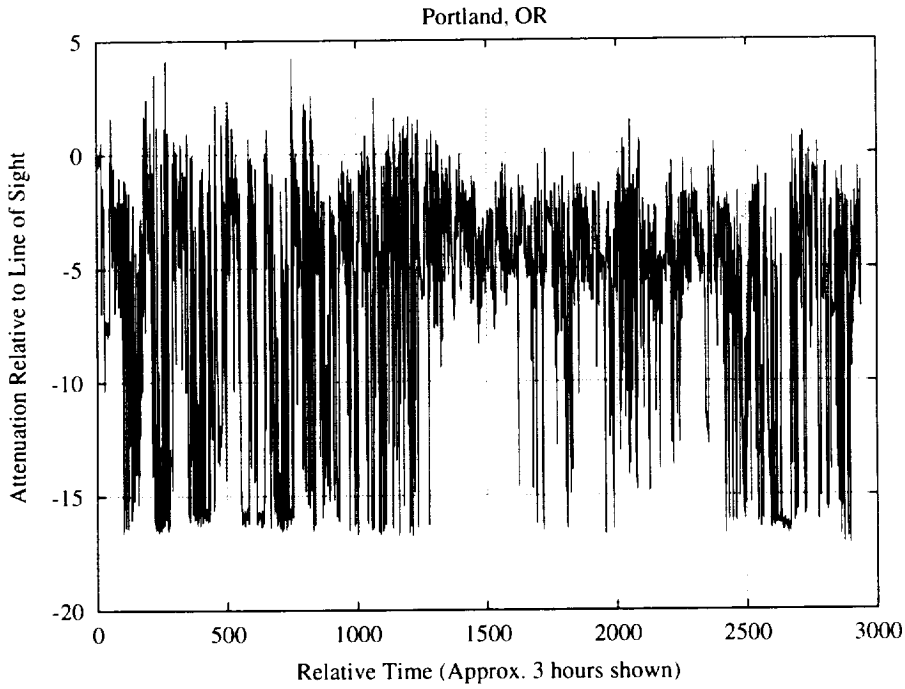
Portland, OR
Attenuation Relative to Line of Sight
5
0
-5
-10
-15
-20
0
500
1000
1500
2000
2500
3000
Relative Time (Approx. 3 hours shown)

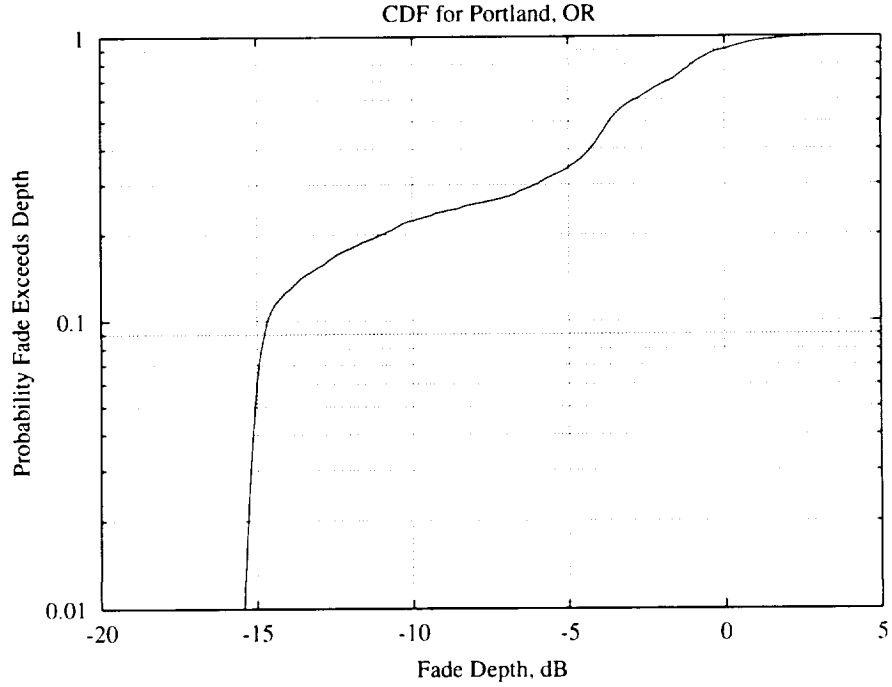
CDF for Portland, OR
Probability Fade Exceeds Depth
1
0.1
0.01
-20
-15
-10
-5
0
5
Fade Depth, dB

San Francisco, CA

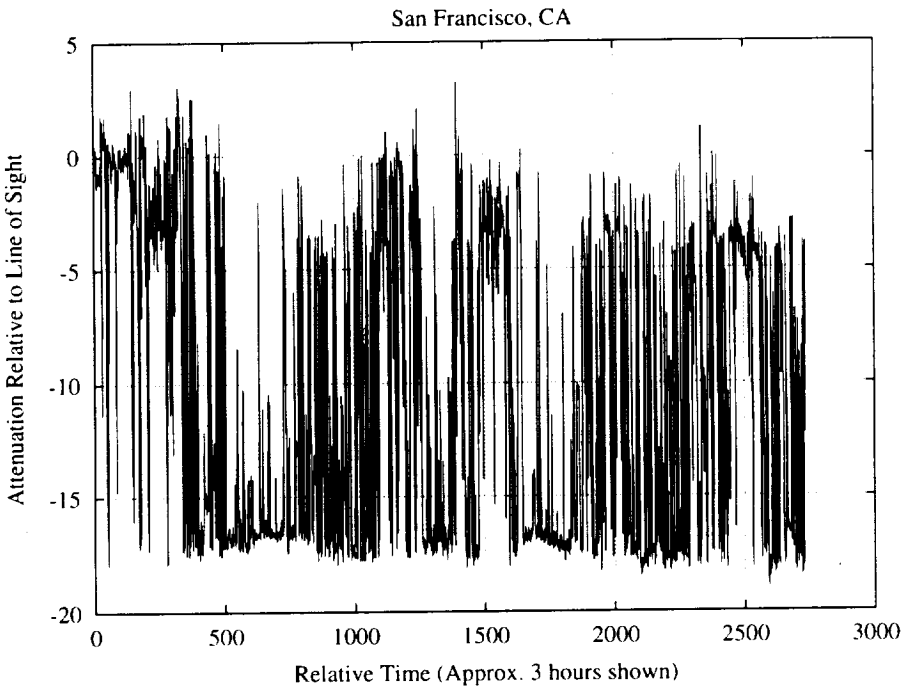

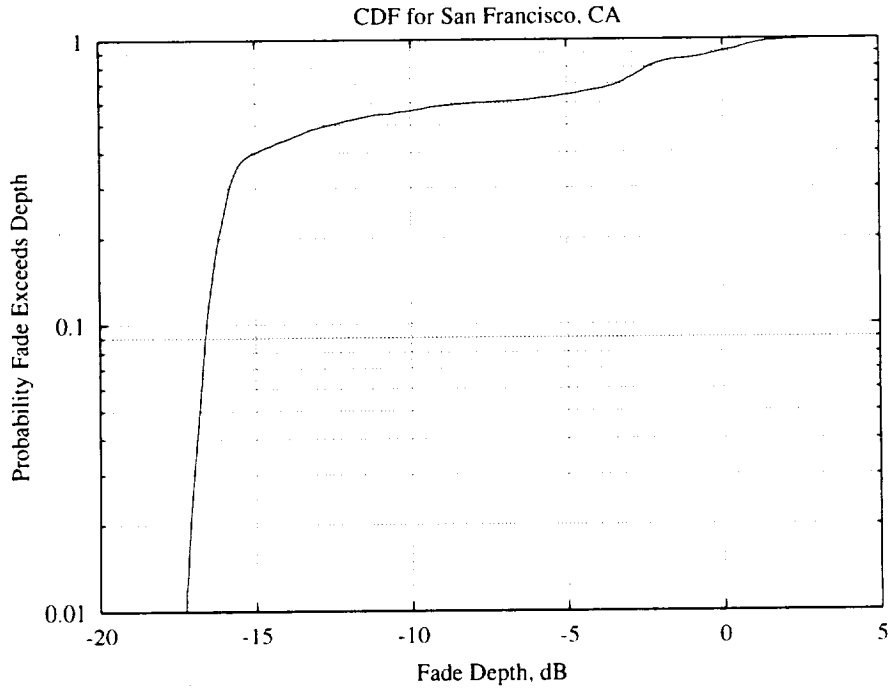

Sequoia National Park

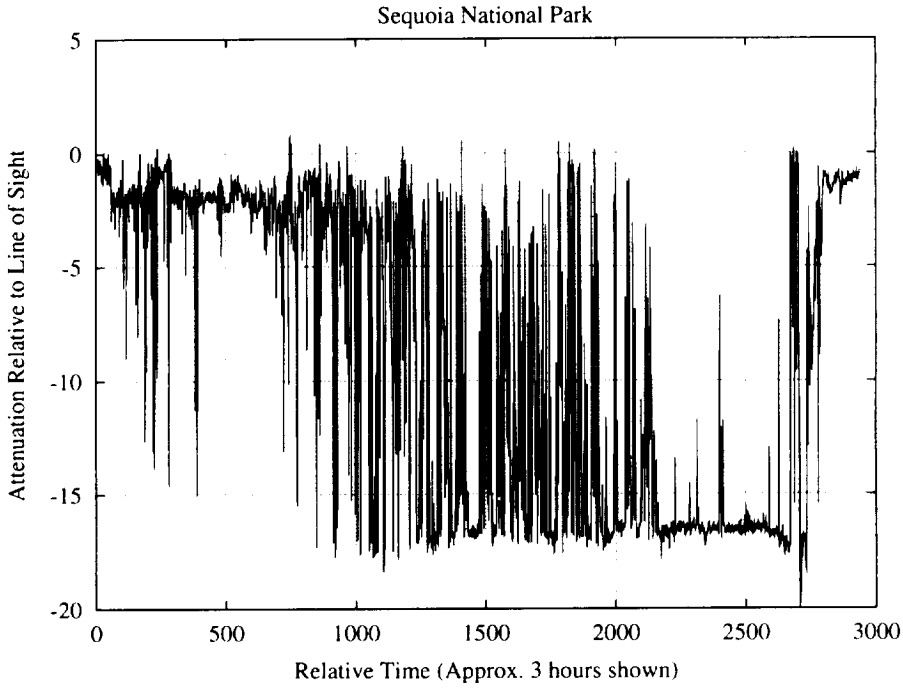

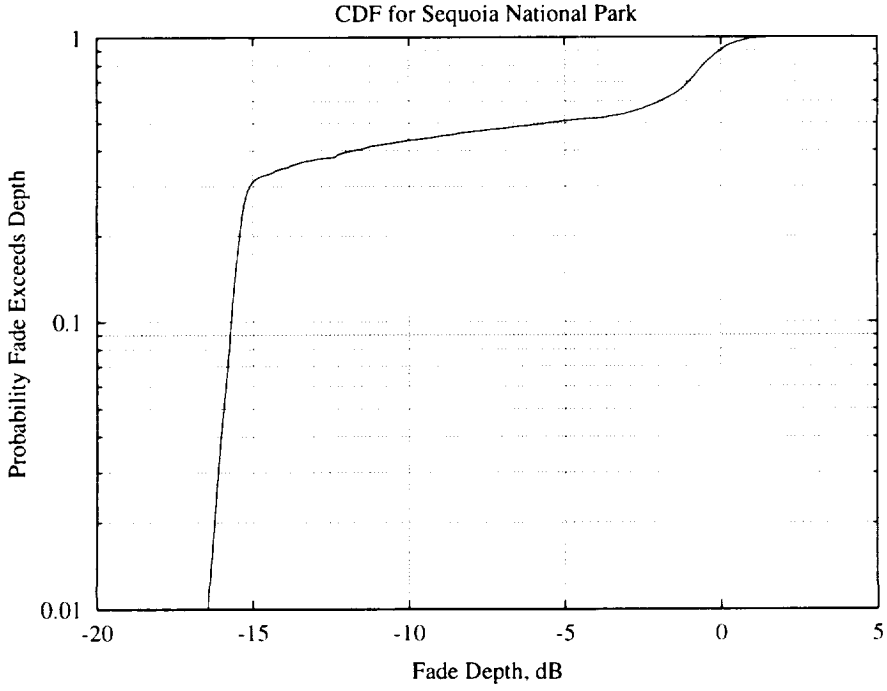

Slidell, LA to Bolton, MS

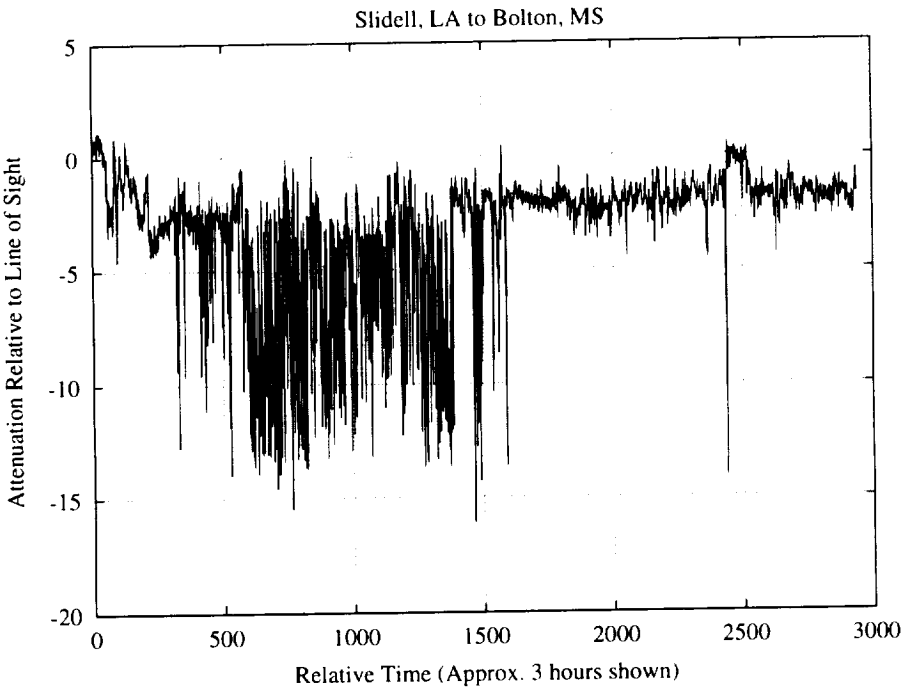

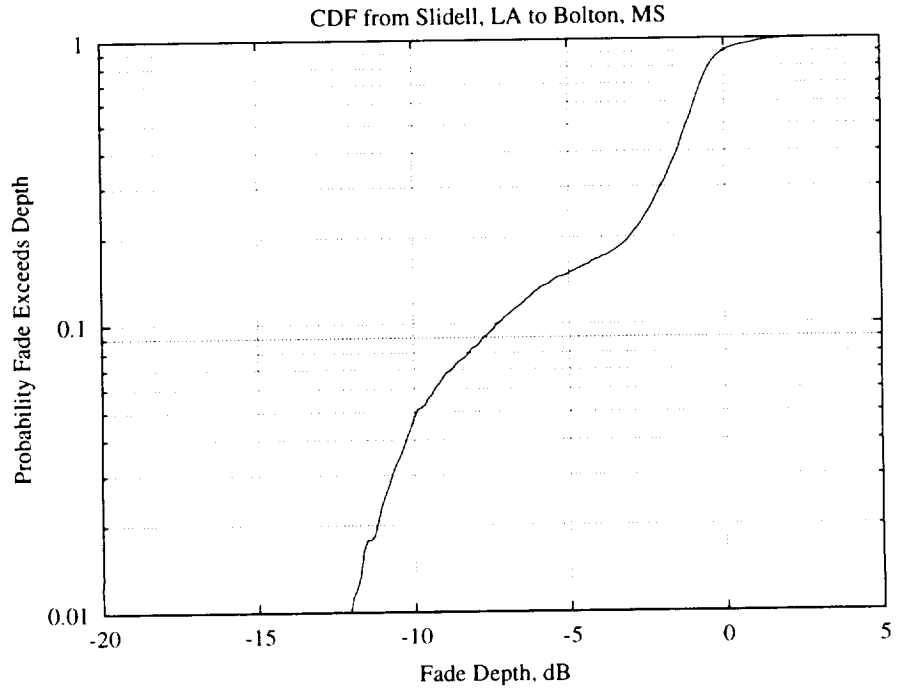

Sonora, TX to Seguin, TX along I-10

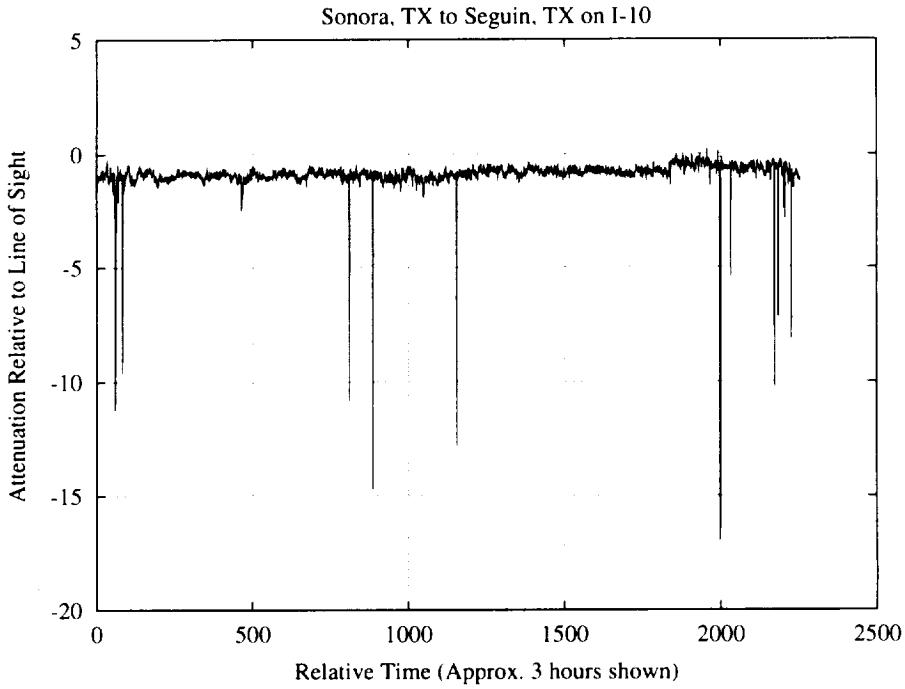

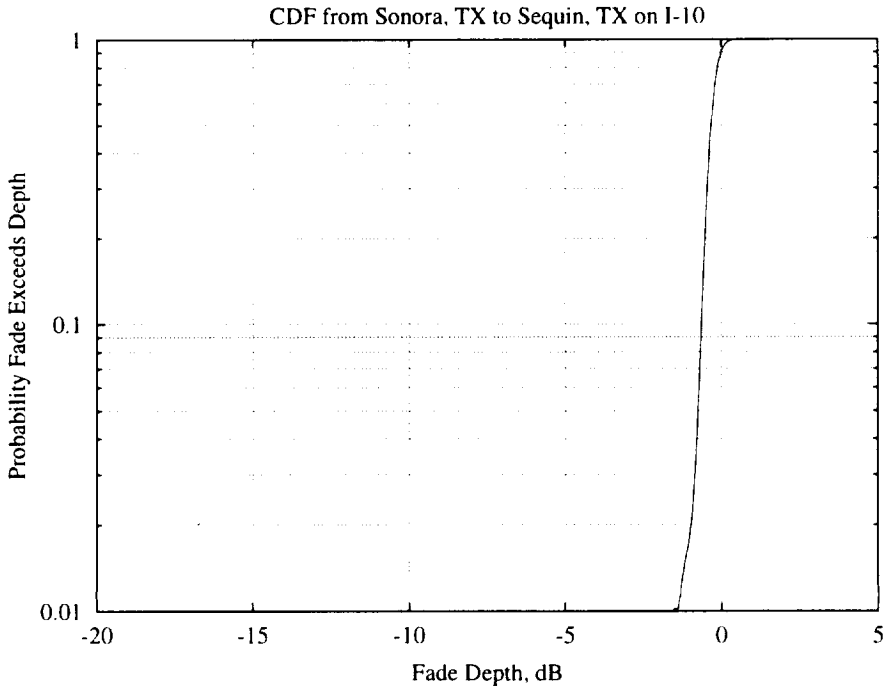

US 180 from Arizona into New Mexico

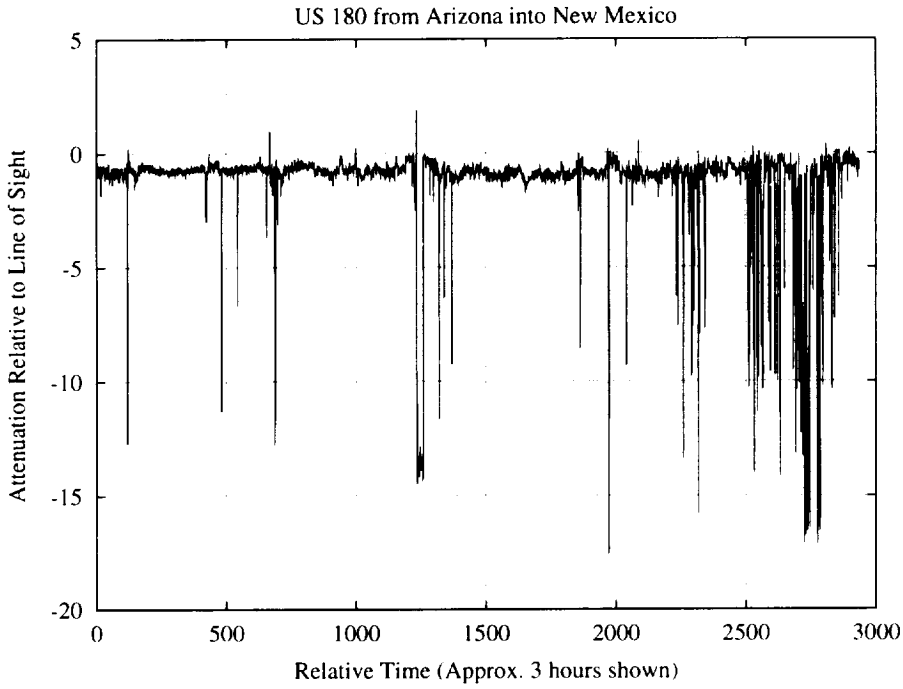

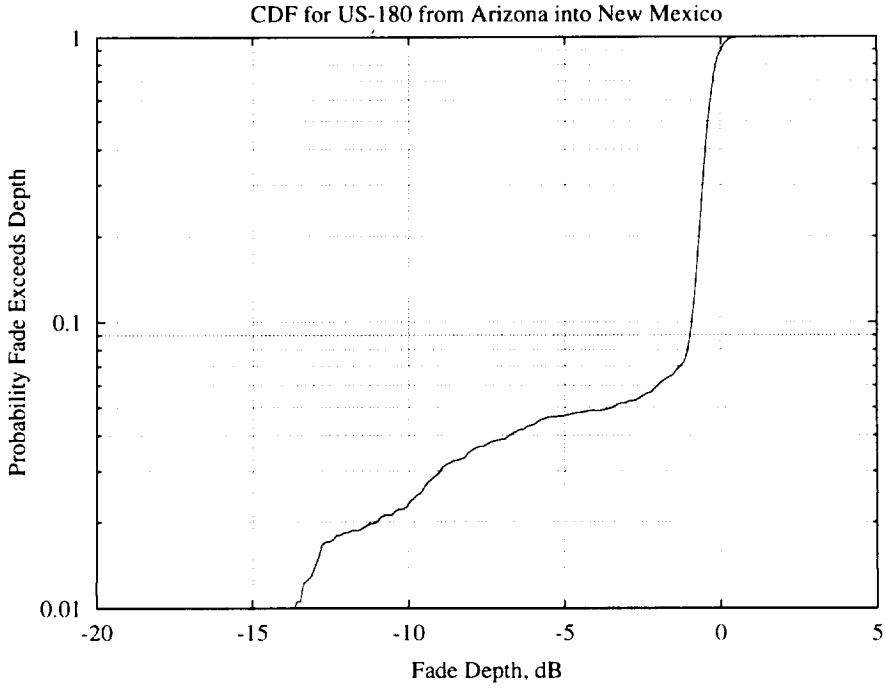

Vicksburg, MS to Pine Bluff, AR

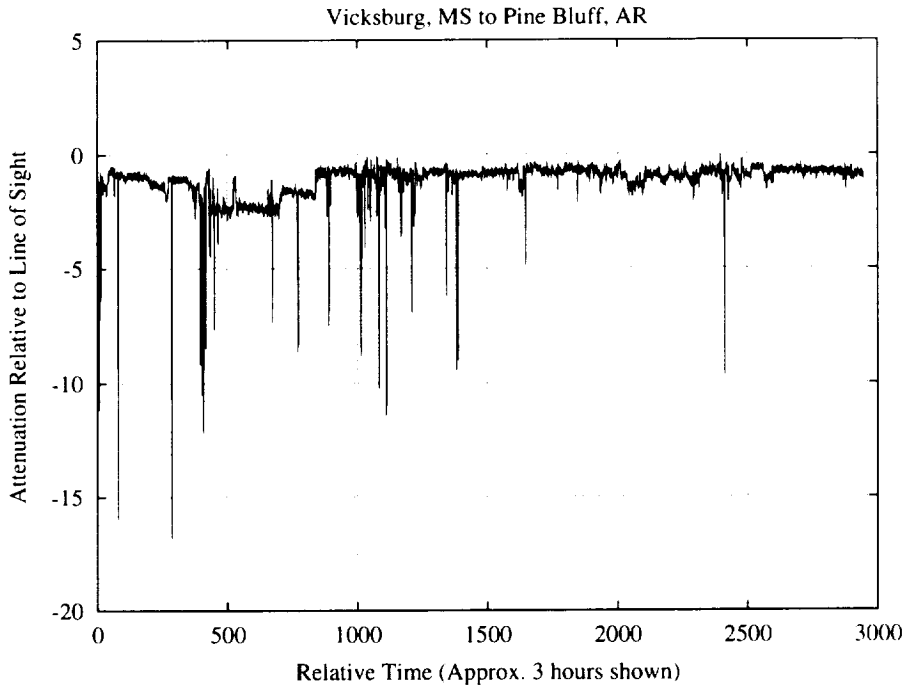

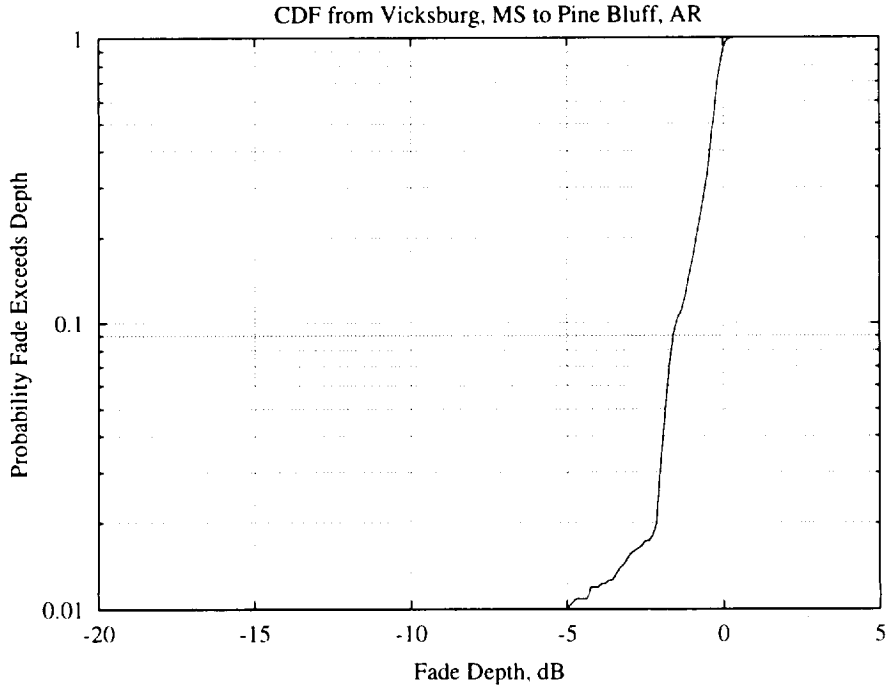

Yosemite National Park

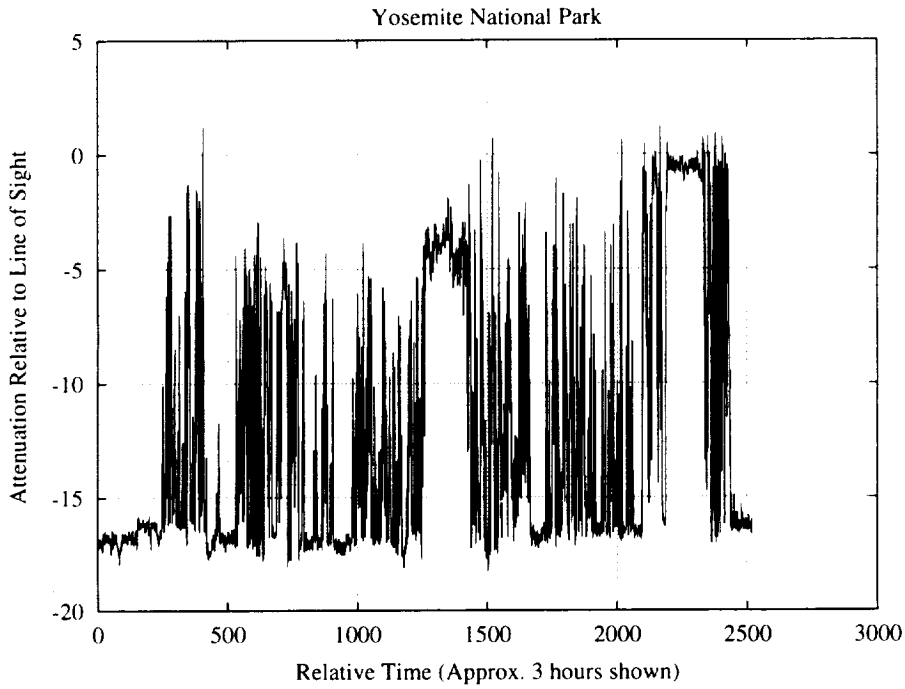

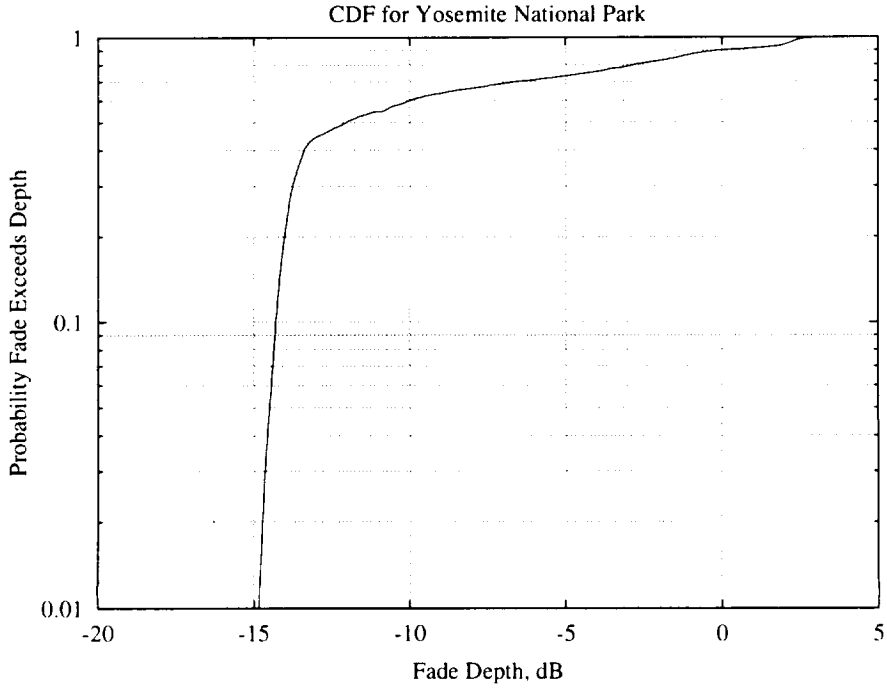

Yellowstone National Park

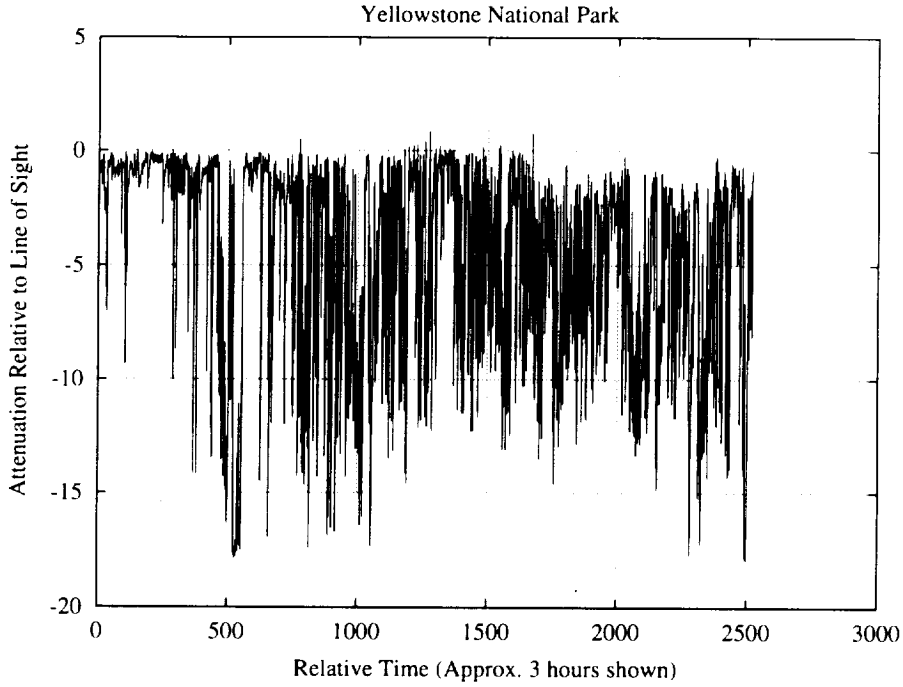

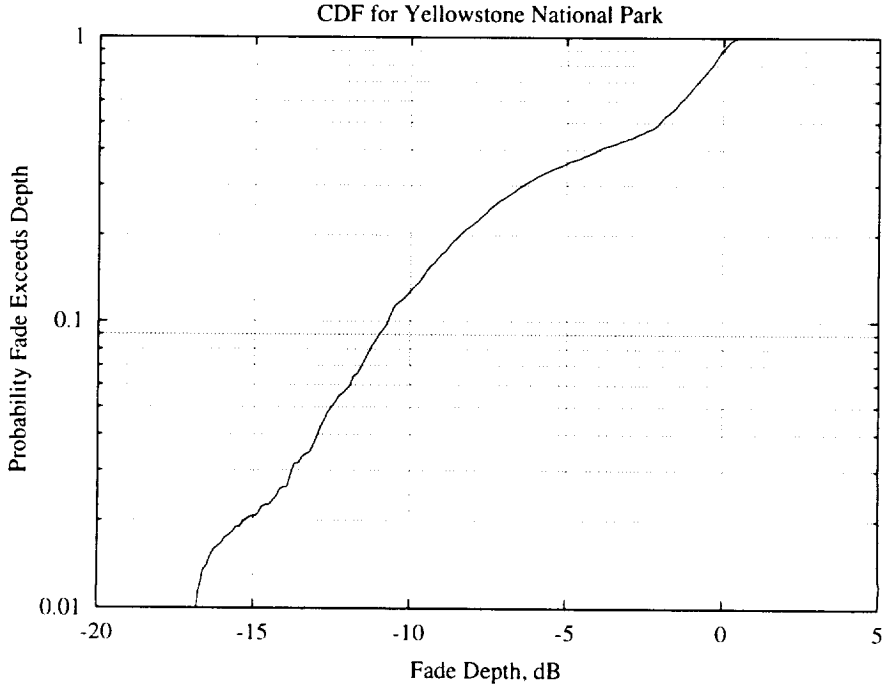

Zion National Park